



# Colored and Fluorescent DOM in the Sea-Surface Microlayer: Response to a Phytoplankton Bloom and Photodegradation in a Mesocosm Study

Claudia Thölen<sup>1</sup>, Jochen Wollschläger<sup>1</sup>, Michael G. Novak<sup>2</sup>, Rüdiger Röttgers<sup>2</sup>, Oliver Zielinski<sup>3</sup>

<sup>5</sup> <sup>1</sup>Institute for Chemistry and Biology of the Marine Environment (ICBM), Carl von Ossietzky Universität Oldenburg, Wilhelmshaven, 26382, Germany

<sup>2</sup>Helmholz-Center hereon, Geesthacht, 21494, Germany

<sup>3</sup>Leibniz-Institute for Baltic Sea Research Warnemünde (IOW), Rostock, 18119, Germany

<sup>10</sup> Correspondence to: Claudia Thölen (claudia.thoelen@uni-oldenburg.de)

**Abstract.** A month long mesocosm study at the Institute for Chemistry and Biology of the Marine Environment (Wilhelmshaven, Germany) examined how a phytoplankton bloom and photodegradation influence colored and fluorescent dissolved organic matter (CDOM and FDOM) in the sea-surface microlayer (SML) and underlying water (ULW). The SML, a thin (<1000  $\mu$ m) interface between ocean and atmosphere, plays a key role in air-sea exchange processes, but temporal mechanisms behind organic matter enrichment remain unclear. To isolate biogeochemical processes from environmental variability, daily SML and ULW samples were analyzed using spectral fluorometric and photometric methods, with supporting data e.g. on irradiance, temperature, and chlorophyll-a. The study covered bloom onset, peak, and decay of two partially overlying phytoplankton blooms. Samples were taken alternatively in the morning and in the afternoon, varying the exposure time to UV-light. Changes in composition and quality of organic matter were tracked using CDOM and FDOM <sup>15</sup> derived parameters. Changes on the FDOM component composition were investigated using PERMANOVA. Protein-like FDOM components increased in both layers during bloom progression, while humic-like FDOM components decreased throughout the study. The significant influence of the bloom phases and the layer (SML or ULW) on the component composition was confirmed, however, their interaction was not significant. It's likely that the change in FDOM component composition is a joint result of the influences of the phytoplankton bloom and photodegradation effects. Based on the slope <sup>20</sup> ratio (SR) of CDOM absorption slopes  $S_{275-295}$  and  $S_{350-400}$ , photodegradation was confirmed as the dominant sink of organic matter over microbial alteration. Generally, photodegradation represented a major sink for aromatic DOM during the mesocosm study, yet its effects were similar in the SML and ULW. Strong vertical mixing, shallow depth, and high light penetration likely prevented surface-specific photochemical gradients from forming.



## 1 Introduction

30 The thin boundary layer between ocean and atmosphere, the sea-surface microlayer (SML), is of high relevance for ocean biogeochemistry and climate-related exchange processes (Cunliffe et al., 2013; Liss and Duce, 1997; Wurl et al., 2011). It plays an important role by influencing climate-related processes (Engel et al., 2017; Wurl et al., 2017), marine carbon cycling (Reinthalter et al., 2008), air-sea gas exchange (Mustaffa et al., 2020), physical surface processes, like wave forming (Gade et al., 2013), and aerosol production (Van Pinxteren et al., 2017; Wilson et al., 2015). Hunter (2009) has defined this  
35 layer by having distinct physical and chemical properties to the underlying water (ULW). Specific compounds in the SML are often enriched due to physical accumulation from the ULW, *in situ* production, or atmospheric deposition (Cunliffe et al., 2013). Literature shows that an SML enriched in organic matter (OM) is known to hinder gas, light, momentum, and heat exchanges between ocean and atmosphere (Cunliffe et al., 2013; Engel et al., 2017; Wurl et al., 2017). A disrupted SML can be reestablished within minutes (Jaeger et al., 2025). Rising air bubbles play a main role as a transport mechanism of  
40 surface-active OM (Hardy, 1982), which also include dissolved OM (DOM).

DOM is one of the most complex and heterogeneous organic mixtures, representing the largest pool of reduced carbon on earth and playing an important role in biogeochemical processes of aquatic environments (Dittmar and Stubbins, 2014; McCarthy et al., 1993). DOM is generally identified as OM produced by natural metabolic processes of plants and animals, passing through a filter with the pore size of 0.2-0.4  $\mu\text{m}$  (Nelson and Siegel, 2013). Absorption and fluorescence spectra of  
45 DOM allow implications about its molecular weight (Peuravuori and Pihlaja, 1997), production (Coble, 1996), composition (Drozdowska et al., 2017; Stedmon and Bro, 2008), transformation and degradation processes. It can serve as a tracer for photochemical and biological processes (Coble, 1996; Repetea and Aluwihare, 2024). Colored DOM (CDOM) has an exponentially decreasing absorption spectra in the ultraviolet (UV)-visible region which changes based on its composition. In coastal waters, terrestrial inputs typically decrease the spectral slope (S), whereas new productivity or intense  
50 photodegradation increases it (Moran and Zepp, 1997). Together with other coefficients, spectral slopes are commonly used to characterize CDOM transformation processes such as photodegradation and microbial alteration (Coble, 2013; Rickard et al., 2022). Specific DOM can emit fluorescence after absorbing the excitation light, hence fluorescent DOM (FDOM). Distinct fluorophores are associated with microbial activity and autochthonous production or more refractory FDOM produced by degradation processes or terrestrial input (Coble, 2013; Kowaleczuk et al., 2013; Nieto-Cid et al., 2006). These  
55 bio-optical methods offer a fast and sensitive way to track short-term dynamics of relevant biological and chemical drivers behind DOM enrichment in the SML (Stramski et al., 2019).

Pathways of CDOM and FDOM from the ULW into the SML or vice versa have been researched in the past but are yet to be investigated on short temporal and spatial scales. CDOM exhibits surface-active properties Blough (1997) and Obernosterer et al. (2005) as well as others (Drozdowska et al., 2017; Miranda et al., 2018; Tilstone et al., 2010; Wurl et al., 2009; 60 Zäncker et al., 2017) report a frequent enrichment of CDOM concentration in the SML compared to the underlying water. Similar trends in FDOM have been identified, where Frew et al., (2002) have reported correlations of surface-active



substances and FDOM concentrations in the SML and ULW. FDOM measurements in the Yellow Sea and East China Sea imply a continuous supply of OM from the ULW into the SML (Yang et al., 2022). In their study, Galgani and Engel (2016) reported a local microbial release of DOM directly in the SML as a response to light exposure. They suggested that a net 65 DOM production in the SML may take place independently of the biological productivity of the underlying waters as a sole microbial response to light exposure. Phytonuston and bacteria are known to inhabit the SML and shape its biofilm like features (Hardy, 2009; Hardy and Apts, 1984; Obernosterer et al., 2005; Reinthaler et al., 2008; Wurl et al., 2016). Phytoplankton produce biopolymers and exude OM, enriching the sea-surface microlayer with surface-active compounds, thus, phytoplankton blooms lead to an enrichment of OM in the SML (Barthelmeß and Engel, 2022; Wurl et al., 2016, 2018). 70 In a mesocosm study, conducted by the BASS (Biogeochemical Processes and Air-Sea Exchange in the Sea-Surface Microlayer) DFG research group (Bibi et al., 2025a), the effects of an induced phytoplankton bloom on the SML and ULW were investigated. It was hypothesized that the CDOM and FDOM signatures in the SML and ULW provide information on the transformation processes of DOM and differ considerably between the two layers.

Energy-rich radiation, such as UV-light, can break apart and degrade DOM into smaller fractions (Zepp et al., 1998). As the 75 SML is directly exposed to elevated solar radiation, photochemical degradation processes of OM play an important role for the biogeochemical processes within the SML (Blough, 1997). Because surfactants affect the radiation penetration depth (Carlucci et al., 1985), the biofilm-like matrix of the SML may also serve as UV protection for microbial and planktonic life in the ULW (Tilstone et al., 2010; Wurl et al., 2016). As water itself absorbs sunlight, also in the UV spectrum (Mason et al., 2016), and the water constituents, such as CDOM add to the UV-light absorption in the water column, the photodegradation 80 strength presumably decreases over depth. On the open sea some studies have found differences in the photodegradation of DOM in the SML and the ULW (Drozdowska et al., 2017; Galgani and Engel, 2016; Miranda et al., 2018; Yang et al., 2022), however Drozdowska et al. (2017), Miranda et al. (2018) and Yang et al. (2022) sampled the ULW at depths  $\geq 1$  m. During the mesocosm study, the ULW was sampled at  $< 1$  m depth to better capture the influence of sunlight on DOM 85 dynamics in the uppermost water layer, similar to Galgani and Engel (2016). The expectation and hypothesis were that photodegradation during the mesocosm study affects the DOM in the SML more than in the ULW, especially regarding the production of OM during the phytoplankton blooms.

Heterogeneity and dynamics in the open sea make it difficult to differentiate between transport processes, environmental 90 drivers, and biogeochemical processes. Mesocosm studies provide controlled conditions that are difficult to achieve in field settings. In the study described here, external sources of DOM such as wet atmospheric deposition and inflow were excluded. Within the enclosed system, potential sources of DOM for the SML included the induced phytoplankton bloom, microbial activity, dry deposition, evaporation, and mixing with the underlying water (Figure 1). Observable sinks included photodegradation and microbial consumption. Of these, the induced phytoplankton bloom (as a source) and photodegradation (as a sink) were chosen to form the focus of this study. The primary objective was to use high-resolution 95 observations of bio-optical properties (absorption and fluorescence) to assess DOM transformation in the SML relative to the ULW.

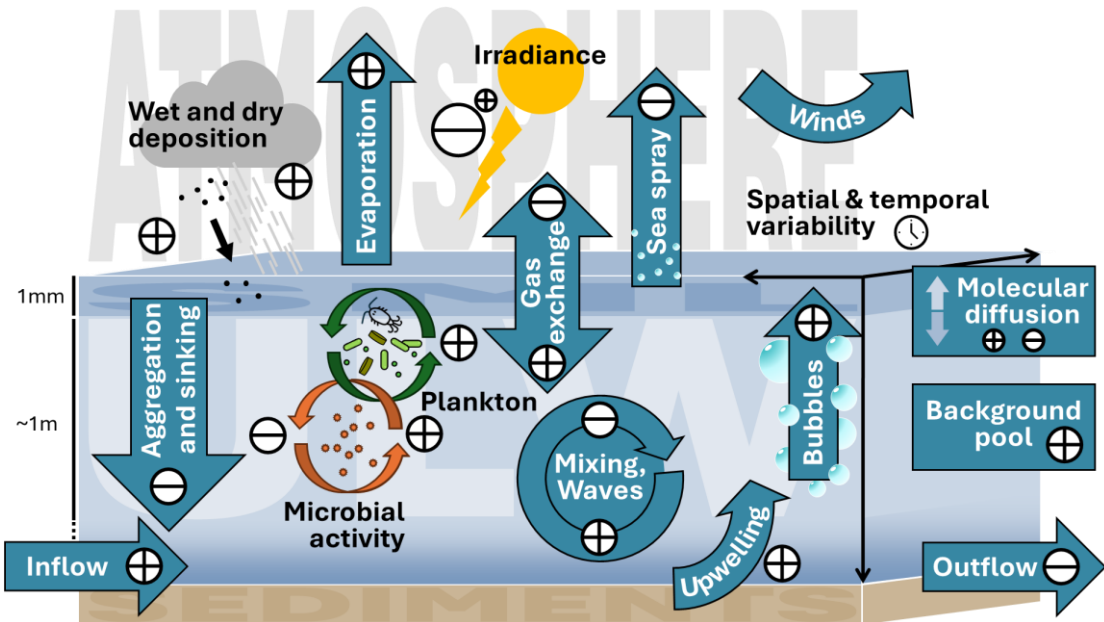


**Figure 1: Pathways and processes of sources (+) and sinks (-) of colored and fluorescent dissolved organic matter into the sea-surface microlayer.**

## 2 Methods

### 100 2.1 Mesocosm study

The mesocosm study was conducted for a month in May and June of 2023 in the Sea Surface Facility (SURF) of the Institute of Chemistry and Biology of the Marine Environment (ICBM) in Wilhelmshaven, Germany. The facility contains an 8 m × 1.5 m × 0.8 m large outdoor basin with a retractable roof, which was closed at night and during rain events. The basin was filled with North Sea water from the adjacent Jade Bay. Homogeneity of the ULW in the basin was achieved by constant mixing of the water column. The daily SML and ULW samples were collected alternating in the morning, about 1 h after sunrise (morning samples, AM), and in the afternoon, about 10 h after sunrise (afternoon samples, PM). The alternation of sampling times intended to capture a potential effect of sun-exposure duration on DOM transformations and elucidated the day and night variability of the layers. The SML was collected via glass plate sampling (Cunliffe and Wurl, 2014). The ULW was sampled via a submerged tube and a connected syringe suction system in 0.4 m depth. The removed sample volume was refilled with Jade Bay water every day. Next to the SURF basin, an irradiance radiometer (Ramses, TriOS, Germany) was mounted on a pole and measured continuously for the wavelengths between 319-956 nm in a 1 min interval. Chlorophyll-a as proxy for phytoplankton biomass was constantly measured in the ULW with a fluorometer (Cyclops 7, Turner Designs, USA) integrated into a FerryBox (4h-Jena, Germany) at approx. 0.4 m depth. From the collected ULW samples, concentrations of chlorophyll-a and other pigments were quantified via high performance liquid chromatography (HPLC) and used to calibrate the continuous FerryBox chlorophyll-a fluorescence measurement.



The available SML sample volume was insufficient for HPLC analysis. However, chlorophyll-a concentrations could be estimated from Quantitative-Filter-Technique Integrating-Cavity Absorption-Meter (QFT-ICAM, (Röttgers et al., 2016)) measurements via the absorption line height at around 670 nm (Roesler and Barnard, 2013; Wollschläger et al., 2014). Additionally, the absorption of non-algal particles (NAP) was deducted by the particulate absorption at 750 nm in the QFT-120 ICAM for SML and ULW. Multiple CTDs (conductivity, temperature and depth, Sea & Sun Technology, Germany) were placed around the basin in different depths to constantly record temperature and salinity. A FlowCam (Yokogawa Fluid Imaging Technologies, USA) was used to quantify and identify particles via imaging. Bacterial abundance was measured every 3<sup>rd</sup> day, because of the large sample volume needed. Surfactants were measured every day for SML and ULW. For a more detailed description of the study setup and its parameters please refer to Bibi et al. (2025a).

## 125 2.2 CDOM and FDOM analysis

The SML and ULW samples were divided into smaller subsamples for the different analyses of all involved groups. 80 ml of each sample were filtered through pre-flushed 0.7 µm Whatman GF/F and 0.2 GHP membrane filters for CDOM and FDOM analysis (40 ml each).

The CDOM samples were stored dark in pre-combusted brown bottles at 4 °C until measurement within weeks of the study. 130 CDOM absorbance was measured from 200-700 nm with three liquid waveguide capillary cells (LWCC, WPI, USA) of different pathlengths (10 cm, 50 cm, 250 cm) to increase the measurement sensitivity following the protocol of Röttgers et al. (2024) using a spectral detector (Model 1310076U1, Avantes, Netherlands). The blank-corrected absorbance spectra were converted into Napierian absorption coefficients (Bricaud et al., 1981).

The FDOM samples were filtered into clear 40 ml SUPELCO bottles. Before use, these bottles were acid-washed twice and 135 combusted at 500 °C for 5 h following the protocol of Ferdinand (personal communication). The samples were stored dark at 4 °C and measured within a few months of the study. FDOM excitation-emission matrices (EEMs) were obtained using an Aqualog (HORIBA, Jobin Yvon, Japan) with a 10 s integration time, high CCD gain, an excitation range from 240-500 nm, and an emission range on the CCD chip from 209-619 nm. The Aqualog measures fluorescence as well as absorption. The resulting data includes an EEM of the blank (purified water standard cuvette, Starna, Type: 3/Q/10/WATER), an EEM of the 140 sample, and the absorption coefficients of the sample. The raw exported Aqualog data was corrected for errors and lamp shifts, by moving the entire EEM spectra for 3 nm on the emission axis, as the water Raman signal of 350 nm was detected at 394, instead of 397. Additionally, single emission spectra were corrupted by showing periodical peaks which were removed by deleting this emission spectra and integrating over it to regain the values at this emission. The corrected EEMs were decomposed by PARAFAC (Murphy et al., 2013) for their underlying fluorophore components using the drEEM and 145 NWAY toolbox (version 0.6.5) in MATLAB (R2020b). The script was adapted following the recommendation of Murphy et al. (2013, supplementary material, appendix A). Before running PARAFAC, the respective blank measurement was subtracted from the sample measurement and the resulting EEM was corrected for the inner-filter effect (IFE, Kothawala et al., 2013; Parker and Rees, 1962, Eq. 1),



$$F_{\lambda_{ex},\lambda_{em}}^{corr} = F_{\lambda_{ex},\lambda_{em}}^{obs} \times 10^{(0.5 \times (A_{\lambda_{ex}} + A_{\lambda_{em}}))}, \quad (1)$$

150 where  $F_{\lambda_{ex},\lambda_{em}}^{obs}$  is the observed fluorescence intensity at an excitation and emission of  $\lambda_{ex}, \lambda_{em}$  nm,  $A_{\lambda_{ex}}, A_{\lambda_{em}}$  are the absorption values at  $\lambda_{ex}, \lambda_{em}$  nm, and  $F_{\lambda_{ex},\lambda_{em}}^{corr}$  is the corrected fluorescence intensity at an excitation and emission of  $\lambda_{ex}, \lambda_{em}$  nm. The fluorescence intensity of the corrected EEM is normalized by using the Raman scatter peak of water, following Eq. 2,

$$F_{\lambda_{ex},\lambda_{em}}(RU) = \frac{F_{\lambda_{ex},\lambda_{em}}^{corr} (AU)}{A_{rp}}, \quad (2)$$

155 where  $F_{\lambda_{ex},\lambda_{em}}(RU)$  is the fluorescence intensity in Raman Units (RU),  $F_{\lambda_{ex},\lambda_{em}}^{corr}$  is the IFE-corrected fluorescence intensity in arbitrary units (AU) and  $A_{rp}^{\lambda_{ex}}$  is calculated as shown in Eq. 3 (Lawaetz and Stedmon, 2009).

$$A_{rp}^{\lambda_{ex}} = \int_{\lambda_{em}^1}^{\lambda_{em}^2} I_{\lambda_{em}} d\lambda_{em}, \quad (3)$$

160 where  $A_{rp}^{\lambda_{ex}}$  is the integral of the Raman peak and  $I_{\lambda}$  is the measured spectrally corrected intensity of the Raman peak at emission wavelength  $\lambda$ . Lawaetz and Stedmon (2009) recommend using the Raman peak of an excitation of 350 nm and an emission of 371 to 428 nm.

The PARAFAC routine first handles the Rayleigh and Raman scatter, masking both from the EEM and interpolating the now blank spaces. The data was first normalized and then examined for outliers by using the *outliertest*-function. Four out of 64 samples were excluded due to exceptionally high fluorescence intensities in the protein-like area of the EEM. A 4-component model was validated with the validation style S4C6T3 for the split half analysis with nonnegativity constraints 165 and  $1^{-8e}$  as the convergence criteria with 50 random starts and a maximum number of 2500 iterations. The resulting final model had a core consistency of 82.04 and the explained percentage was 99.54 %. The model was then uploaded to OpenFluor (Murphy et al., 2014) and used to find similar fluorophores in published datasets.

Established indices like the humification index (HIX, Zsolnay et al., 1999) and the biological index (BIX, Huguet et al., 2009) require the total fluorescence intensity of a set pair of excitation and emission wavelengths. Therefore, the corrected 170 EEMs were preconditioned just like for the PARAFAC analysis but were then used to calculate HIX and BIX in a custom MATLAB routine. A variety of indices and ratios can be derived from FDOM fluorescence intensity serving as proxies for DOM molecular weight, source, and state (Álvarez-Salgado et al., 2023; Hansen et al., 2016; Huguet et al., 2009; Zsolnay et al., 1999). From the established indices, those that have previously been applied to coastal waters and are applicable to aid in answering the proposed hypotheses are used in this study, for an overview please refer to Table 1. Parameters which are 175 calculated by using specific FDOM components are created by using the PARAFAC derived versions of these components. E.g.: Coble (1996) describes the fluorescence at an excitation of 312 nm and an emission of 380-420 nm as peak M, marine humic-like fluorescence. Based on the mesocosm PARAFAC results the equivalent to this component peaked at an



excitation of 312 nm and an emission of 405 nm. The intensity value at this peak was used for the calculation of any literature-based indices including peak M.

180

**Table 1: CDOM and FDOM derived parameters. If specific literature based FDOM components are used for the original calculation they are translated into the PARAFAC derived components of this study.  $I_{\lambda ex, \lambda em}$  is the fluorescence intensity at the given wavelengths.**

Parameter based on literature	Calculation based on PARAFAC components and absorption coefficients	Reference	Purpose and interpretation
<b>FDOM derived parameters</b>			
Humification index (HIX)	$\frac{\sum I_{ex254,em480}}{\sum I_{ex254,em435}}$	Zsolnay et al., 1999	Indicator of humification: High values correspond to a high degree of aromaticity and indicate the presence of complex molecules.
Biological index (BIX)	$\frac{I_{ex310,em380}}{I_{ex310,em430}}$	Huguet et al., 2009	Indicator of autotrophic productivity: Increases with the accumulation of marine humic-like fluorophores and reflects freshly produced DOM and photoautotrophic microbial by-products in samples. High BIX values ( $>1$ ) indicate predominantly autochthonous, freshly released DOM, while lower values (0.6-0.7) suggest reduced DOM production
Recently produced index (REPIX)	$\frac{I_{C1} + I_{C3}}{I_{C2}}$	Drozdowska et al., 2013	Distinguishes freshly produced FDOM based on microbial activity. High values ( $>1$ ) indicate autochthonous FDOM, low values ( $<0.6$ ) allochthonous origin, and intermediate values (0.6-1.0) low DOM production.
T/M	$\frac{I_{C3}}{I_{C1}}$	Romera-Castillo et al., 2010	A lower value indicates a dominance of respiration products over products by healthy marine phytoplankton.
<b>CDOM and FDOM derived parameters</b>			
M/a325	$\frac{I_{C1}}{a312}$	DeHaan, 1993; Lønborg et al., 2010	The ratio indicates which fraction of the absorbed light is being re-emitted as fluorescence. A higher ratio suggests that the marine humic-like substances are more humified or less photodegraded.
<b>CDOM derived parameters</b>			
Slope ratio (SR)	$SR = \frac{S_{275-295}}{S_{350-400}}$	Helms et al., 2008	The SR is correlated with DOM molecular weight (MW) and to photochemically induced shifts in the MW. Photochemical degradation of terrestrial DOM leads to an increase in the absolute value of the SR.
a254 [m <sup>-1</sup> ]	$a254$	Summers et al., 1987; Weishaar et al., 2003	Absorbance at 254 nm is commonly used as a proxy for dissolved organic carbon (DOC) concentration and aromaticity as aromatic and conjugated structures strongly absorb UV light in this range. High values correspond to high aromaticity.
a440 [m <sup>-1</sup> ]	$a440$	Kirk, 1983	Absorbance at 440 nm is commonly used as a proxy for CDOM concentration in the visible range of the CDOM spectra.



## 2.3 Statistics

185 To test if the phytoplankton bloom phase and other environmental variables had significant influences on the FDOM component composition in the SML and the ULW, a two-way PERMANOVA (PERmutational Multivariate ANalysis of Variance) was performed in RStudio (Version 1.4.1103) with 9999 permutations and the “bray” method for the distance matrix. PERMANOVA is a non-parametrical multivariate test for variations among groups compared to the variations within a group (Anderson, 2001). For visualization a non-metric multidimensional scaling (nMDS, Clarke, 1993) plot was created  
190 using the same distance matrix as for PERMANOVA.

195 To compare selected variables between the SML and ULW, differences in the layer means were assessed using paired t-tests or Wilcoxon signed-rank tests depending on normality (Lilliefors, 1967). Temporal trends were quantified via linear regression to obtain slopes and R<sup>2</sup> values, and differences in slopes were evaluated using linear mixed-effects models with day as a random effect (Pinheiro and Bates, 2000). Variability between layers was tested using a robust Brown-Forsythe approach (Brown and Forsythe, 1974). Bootstrap resampling (n = 1000) provided 95% confidence intervals for differences in R<sup>2</sup> (Efron, 1979). Additionally, the average enrichment factor ( $\bar{\theta}$  EF, Eq. 4), which indicates if a variable is generally higher in the SML ( $\bar{\theta}$  EF > 1) or in the ULW ( $\bar{\theta}$  EF < 1) was calculated for selected variables (Table 5).

$$EF = \frac{I_{SML}}{I_{ULW}}, \quad (4)$$

where  $I_{SML}$  and  $I_{ULW}$  are the intensities of a given variable in the SML and the ULW, respectively.

## 200 3 Results

### 3.1 Environmental variables during the mesocosm study: chlorophyll-a, non-algal particles, temperature, salinity, bacterial abundance, surfactant concentration, and incident light

Since OM transformation processes are influenced by environmental conditions, selected descriptive variables from the mesocosm study are presented here alongside the CDOM and FDOM results.

205 In the ULW, chlorophyll-a concentrations were elevated during the first two days of the mesocosm study, initially exceeding 5  $\mu\text{g L}^{-1}$  before dropping to about 1.2  $\mu\text{g L}^{-1}$  (Figure 2a). After May 22, the concentration gradually increased until the nutrient addition on May 26, which triggered the first bloom peak on May 28. After further nutrient additions on May 30 and June 1, chlorophyll-a reached a second peak on June 3 (11.4  $\mu\text{g L}^{-1}$ ), after which it declined to 1-2  $\mu\text{g L}^{-1}$  within a week.

210 In contrast, chlorophyll-a concentrations in the SML were consistently higher than in the ULW ( $\bar{\theta}$  EF = 49.75). The first measurement on May 20 already showed values around 10  $\mu\text{g L}^{-1}$ , while ULW concentrations had dropped to  $\sim 1 \mu\text{g L}^{-1}$ . SML values continued to rise with a delayed increase relative to the ULW, exceeding 100  $\mu\text{g L}^{-1}$  by May 31. Towards the end of the study, chlorophyll-a concentrations in the SML reached  $\sim 250 \mu\text{g L}^{-1}$ , with a pronounced peak of  $\sim 500 \mu\text{g L}^{-1}$  on June 13. Based on chlorophyll-a dynamics and nutrient availability, three bloom phases were distinguished (Bibi et al., 2025): an onset phase from the beginning of the study until May 27, a peak phase from May 27 to June 5, and a decay phase



215 from June 5 to the end of the study on June 15. According to Bibi et al. (2025a), the first chlorophyll-a peak was dominated by the coccolithophore *Emiliania huxleyi*, one of the most abundant and globally occurring coccolithophore species (Balch, 2018), while the second peak was caused by *Cylindrotheca closterium*, a widely distributed diatom typically found in nutrient-rich coastal waters.

220 Absorption by NAP was consistently higher in the SML than in the ULW ( $\text{Ø EF} = 35.87$ ), with particularly elevated values during the bloom and decay phases (Figure 2b). Chlorophyll-a and NAP were significantly correlated in the SML but not in the ULW (Figure A1).

225 Temperature and salinity values at 0.4 m depth in the mesocosm basin both generally increased during the study. While the temperature showed diurnal changes, it rose from about 17 °C on May 18 to about 24 °C on June 16, as summer was progressing in Germany. The salinity increased almost linearly from about 29.3 to 32.2 PSU in the same period (Figure 2c), due to evaporation.

230 Bacterial abundances ranged between  $\sim 2.5 \times 10^8$  and  $1.7 \times 10^9$  cells L<sup>-1</sup> in the ULW and between  $\sim 4.8 \times 10^8$  and  $1.5 \times 10^9$  cells L<sup>-1</sup> in the SML (Figure 2d). Overall, no significant difference in free-living bacterial cell numbers between the two layers was observed. However, temporal variations followed the phytoplankton bloom development, with lower cell numbers around the bloom peak and higher abundances in the post-bloom phase. A detailed description of bacterial dynamics during the study is provided in Bibi et al. (2025a) and Athale et al. (in prep).

Data for the surfactant concentration was provided by Bibi et al. (2025a, b). In Figure 2e, a clear distinction between SML and ULW is visible, as the SML is almost always enriched in surfactants ( $\text{Ø EF} = 3.32$ ). The development of surfactants in the SML follows the bloom with some delay, while the concentration in the ULW says relatively stable.

235 The integrated incident light from the daily light minimum (approx. midnight) to the sampling time is displayed for each sampling time in Figure 3. Morning samples, which were taken about 1 h after sunrise, were always less irradiated than the afternoon samples, which were taken about 10 h after sunrise. The maximum integrated light exposure for the morning samples was approx.  $4 \times 10^4$  W m<sup>-2</sup>, while maximum incident light of the afternoon samples was approx.  $6 \times 10^7$  W m<sup>-2</sup>. During the first days of the study, May 17 to May 25, there was more variance in the incident light due to cloud coverage and rain events. During rain events the roof of SURF was closed which blocked the UVA partition of the total incident light. 240 From June 5, the incident light during the day was quite similar at high levels of  $6 \times 10^7$  W m<sup>-2</sup> every day until the end of the study.

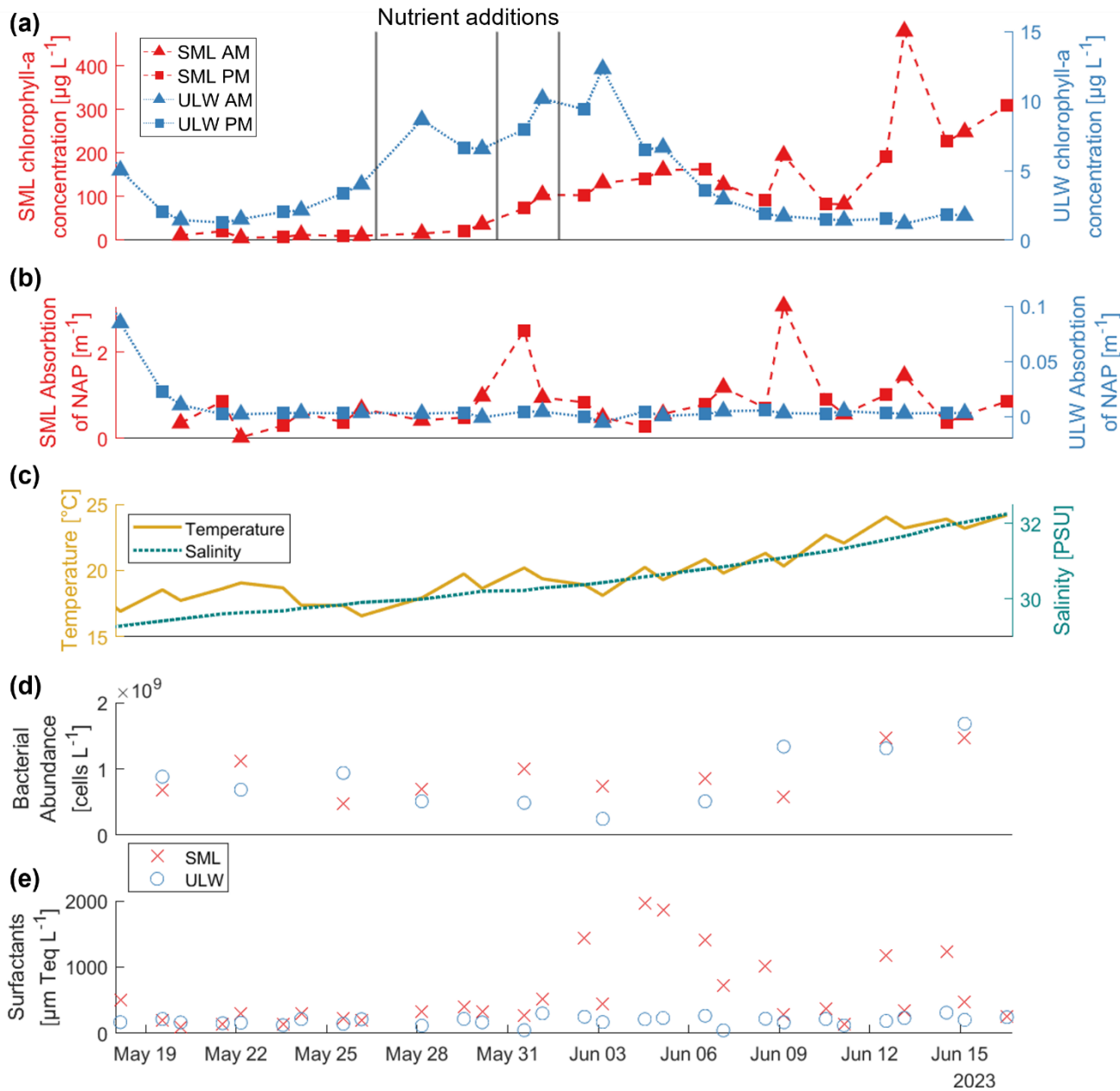
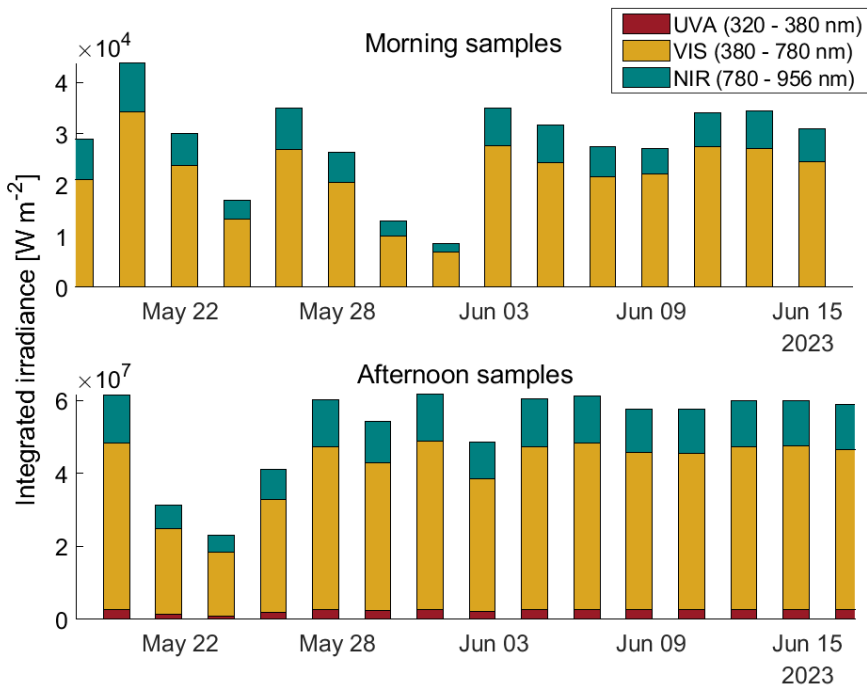


Figure 2: Concentration of chlorophyll-a in  $\mu\text{g L}^{-1}$  (a) and absorption of non-algal particles (NAP) in  $\text{m}^{-1}$  (b) measured via the absorption line height at 670 nm, and the absorption at 750 nm, respectively, on a filter pad (QFT-ICAM, Röttgers et al., 2015) for the sea-surface microlayer (red, left Y-axis) and the underlying water (blue, right Y-axis). Triangles are the morning samples; squares represent the afternoon samples. Nutrient additions are marked as black vertical lines on May 26, May 30 and June 1. (c) Temperature in  $^{\circ}\text{C}$  (yellow, solid line, left Y-axis) and salinity in PSU (green, dashed line, right Y-axis) measured by a CTD (Sea & Sun Technology, Germany) in the mesocosm basin in about 0.4 m depth. (d) Bacterial abundance in  $\text{cells L}^{-1}$  for the sea-surface microlayer (SML, red) and the underlying water (ULW, blue). (e) Surfactant concentrations in  $\mu\text{m Teq L}^{-1}$  (Triton-X equivalent) for the sea-surface microlayer (SML, red) and the underlying water (ULW, blue). Temperature, salinity, bacterial abundance and surfactant data are adapted from Bibi et al. (2025a).

245

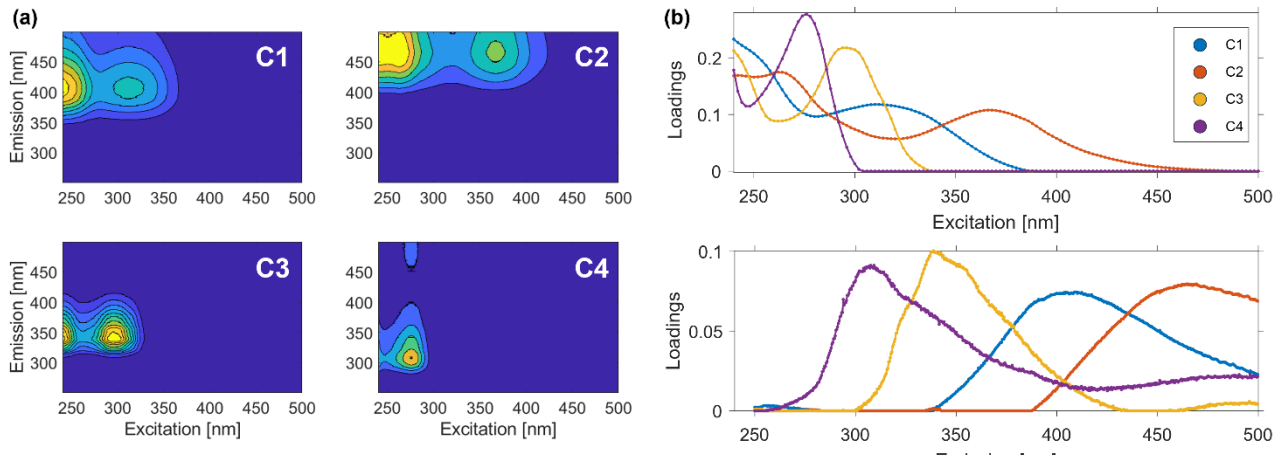
250



255 **Figure 3: Integrated irradiance in  $\text{W m}^{-2}$  measured with a TriOS Ramses irradiance radiometer from midnight of each sampling day until the sampling time. The total measured irradiance range (319-956 nm) is split into its fractions of ultra-violet-A (UVA, 320 to 380 nm, red) visual (VIS, 380 to 780 nm, yellow) and near-infrared (NIR, 780 to 956 nm, teal). Upper panel: integrated irradiance during morning samples (~1 h after sunrise); lower panel: afternoon samples (~10 h after sunrise).**

### 3.2 FDOM PARAFAC results

The validated PARAFAC model initially identified four FDOM components within the mesocosm samples, hereafter named 260 C1, C2, C3 and C4 (Table 2, Figure 4). C1 (Excitation (Ex) <240/312 nm, Emission (Em) 405 nm) corresponds to the marine humic-like peak from Coble (1996, 2007) and is connected to marine phytoplankton, autochthonous production and microbial activity (Chen et al., 2018; Romera-Castillo et al., 2010; Shutova et al., 2014). Component C2 (Ex 264/368 nm, Em 464 nm) had two excitation peaks which are assignable to Coble's humic-like peaks A and C. They both correspond to allochthonous terrestrial DOM (Chen et al., 2021; Shutova et al., 2014; Yang et al., 2022). Baker et al. (2007) bring peak C 265 into connection with fulvic acid while peak A can be more connected with humic acid. C3 (Ex 296 nm, Em 340 nm) and C4 (Ex 276 nm, Em 307 nm) are both protein-like components (Coble, 1996, 2007) corresponding to microbial activity. C3 has been described as tryptophan-like (Calderó-Pascual et al., 2022; Coulson et al., 2022; Eder et al., 2022), and C4 as tyrosine-like (Catalá et al., 2015; Marcé et al., 2021; Walker et al., 2009).



270

**Figure 4:** (a) Excitation-emission-matrices (EEMs) for the fingerprints of the four validated PARAFAC components (C1-C4). (b) Spectral loadings of PARAFAC components, C1 (blue), C2 (red), C3 (yellow) and C4 (purple).

**Table 2:** Validated PARAFAC components (C1-C4) with their excitation and emission wavelength maxima ( $Ex_{max}$ ,  $Em_{max}$ ), their assignment to fluorophores classified in existing literature, the nomenclature created by Coble in 1996 and 2007, their sources and OpenFluor references based on the PARAFAC output as well as other fitting references and their respective components.

275

Component in this study	$Ex_{max}$ [nm]	$Em_{max}$ [nm]	Literature component name (Coble, 1996, 2007)	Sources	References (OpenFluor)
C1	<240/312	405	Marine humic-like (M)	Marine phytoplankton, microbial activity, autochthonous	Chen et al., 2018 (C<260(305)/404); Romera-Castillo et al., 2010 (peak-M); Shutova et al., 2014 (C7)
C2	264/368	464	Humic-like (A, C)	Terrestrial delivered humic-like OM, fulvic acid, soils and suspended particles, allochthonous	Chen et al., 2021 (C2); Shutova et al., 2014 (C1); Yang et al., 2022 (C1)
C3	<240/296	340	Protein-like, tryptophan-like (T)	Marine phytoplankton, microbial activity, autochthonous	Calderó-Pascual et al., 2022 (C2); Coulson et al., 2022 (C4); Eder et al., 2022 (C6)
C4	<240/276	307	Protein-like, tyrosine-like (B)	Marine phytoplankton, microbial activity, autochthonous	Catalá et al., 2015 (C4); Marcé et al., 2021 (C5); Walker et al., 2009 (C5)

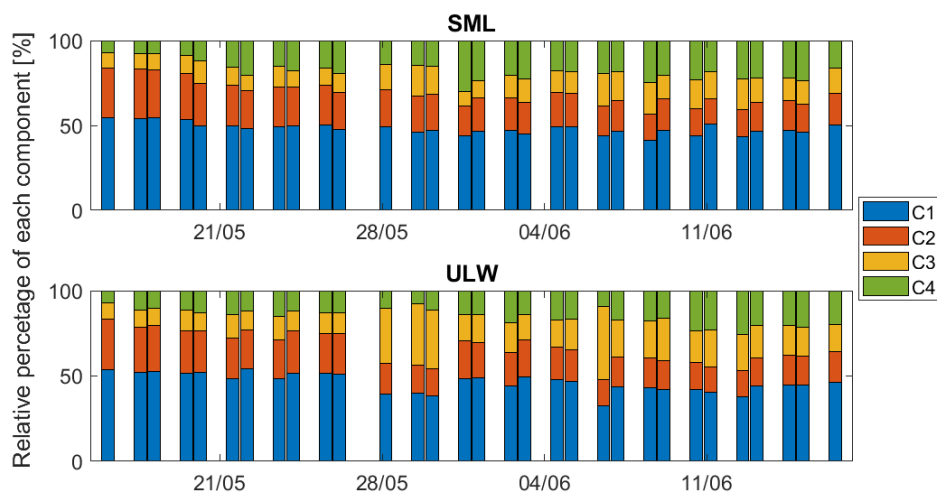
### 3.3 FDOM component composition and bloom sections

Figure 5 shows the relative percentage of PARAFAC components (C1-C4) in each SML and ULW sample. As FDOM is influenced by various environmental sinks and sources (Figure 1), the component composition can provide information on the transformation processes. Component C1 (blue) dominated both layers, accounted for 41-54 % of SML samples and remained relatively constant. In the ULW, C1 was similarly abundant but dropped to ~38 % during the first bloom peak and

280



~32% after the second bloom. C2 (red) contributed 15-29 % in both layers. It reached its lowest relative percentage during the peak phase and increased slightly again towards the end of the study. C3 (yellow) showed the strongest variability. In the SML, it rose from 9 % to 19 % mid-study before declining to ~15 % by the end. In the ULW, C3 peaked during the first bloom (May 28-30) and again on June 6, reaching up to 43 %, before stabilizing at ~20 % in the decay phase. C4 (green) 285 increased steadily throughout the study. Starting at ~7 % in both layers, it rose in the SML to ~30 % during the bloom and then stabilized at ~22 %. In the ULW, C4 increased more gradually, peaking at ~25 % towards the end of the study.



**Figure 5: Relative percentage of PARAFAC components (C1-C4) during the mesocosm study. Upper panel: Sea-surface microlayer (SML). Lower panel: Underlying water (ULW).**

290 To statistically analyze the influence of different environmental variables on the FDOM component composition a PERMANOVA and a follow-up nMDS analysis were performed on the compositional data and its distance matrix. The PERMANOVA results were obtained from two separate runs. Based on the first hypothesis, for the first run, it was tested which influence the layer (SML or ULW) and the bloom phase (onset, peak, decay) had on the FDOM component composition (*Layer*  $\times$  *Phase* run, Table 3). In the second run a set of environmental variables was tested for their influence 295 on the composition (*Environmental variables* run, Table 4).

The results of the *Layer*  $\times$  *Phase* run stated a moderate, but highly significant influence ( $R^2 = 0.49, p < 0.001$ ) of the bloom phase on the FDOM component composition (Table 3). The layer had a significant but negligible influence ( $R^2 = 0.08, p < 0.001$ ) on the composition. The interaction of these two factors, phase and layer, did not have a significant influence ( $p = 0.2993$ ). 42 % of the variation remained unexplained with these two factors.

300 The nMDS plot of the bloom phase and layer for the PARAFAC components showed a separation of the bloom phases with a small stress value of 0.102 (Figure 6). The layers were not clearly separated in the nMDS plot for the onset and peak phase, yet the SML values appeared to be mostly higher in the y-axis. The decay phase showed some separation and clustering of the layer variable.



When the PERMANOVA model was refined by using defined environmental variables it was first tested whether the  
305 available environmental variables were correlated with each other and therefore redundant in the PERMANOVA. Based on a correlation matrix and coefficients of determination ( $R^2$ ) values  $> 0.80$  (data not shown), temperature, salinity, phase, layer and sampling time (AM or PM) were excluded. The PERMANOVA *Environmental variables* run contained the date, UVA-light, surfactants, chlorophyll-a and NAP (Table 4). It was tested whether to include the bacterial abundance into the PERMANOVA, but because of the low number of samples, many days had to be excluded from the analysis not reflecting  
310 the study completely.

In the *Environmental variables* run, the progressing time (Date) explained 48 % of the variation ( $p < 0.001$ ). Influences of NAP and the surfactants (correlating strongly with the layer) were significant and moderately significant ( $p = 0.0034$ ,  $p = 0.0134$ ), respectively. The influence of chlorophyll-a on the FDOM component composition was slightly significant ( $p = 0.0623$ ) and the UVA-light had no significant influence ( $p = 0.1493$ ). From the variable interactions the most notable is  
315 the interaction between the UVA-light, chlorophyll-a and the NAP which had a high significance ( $p = 0.0005$ ) but a small  $R^2$  of 0.046.

320 **Table 3: PERMANOVA results of the *Layer*  $\times$  *Phase* run: coefficient of determination ( $R^2$ ), pseudo-F statistic (F), and p-value.**  
Large F-values mean that the variation between groups is large relative to the variation within groups. Significance codes: highly significant/ $p < 0.001$ : ‘\*\*\*’, significant/ $p < 0.01$ : ‘\*\*’, moderately significant/ $p < 0.05$ : ‘\*’, slightly significant/ $p < 0.1$ : ‘.’, not significant/ $p < 1$ : ‘ns’.

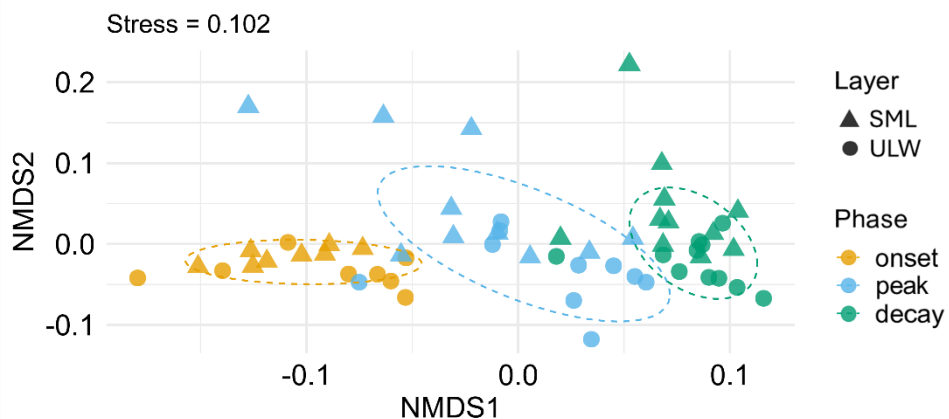
	$R^2$	F	p-value
<b>Layer</b>	0.082	10.497	0.0001 ***
<b>Phase</b>	0.485	61.964	0.0001 ***
<b>Layer <math>\times</math> Phase</b>	0.010	1.230	0.2993 ns
<b>Residual</b>	0.438		

325 **Table 4: PERMANOVA results of the *Environmental variables* run (Date, UVA-light (UVA), surfactants, chlorophyll-a (Chla), non-algal particles (NAP)): coefficient of determination ( $R^2$ ), pseudo-F statistic (F), and p-value.** Large F-values mean that the variation between groups is large relative to the variation within groups. Significance codes: highly significant/ $p < 0.001$ : ‘\*\*\*’, significant/ $p < 0.01$ : ‘\*\*’, moderately significant/ $p < 0.05$ : ‘\*’, slightly significant/ $p < 0.1$ : ‘.’, not significant/ $p < 1$ : ‘ns’. Only the results for the environmental variables themselves and the significant interactions are shown.

	$R^2$	F	p-value
<b>Date</b>	0.484	82.396	0.0001 ***
<b>UVA-light (UVA)</b>	0.011	1.893	0.1493 ns
<b>Surfactants</b>	0.027	4.563	0.0134 *
<b>Chlorophyll-a (Chla)</b>	0.017	2.859	0.0623 .
<b>Non-algal particles (NAP)</b>	0.038	6.424	0.0034 **
<b>Surfactants <math>\times</math> NAP</b>	0.018	3.124	0.0502 .



<b>Chla × NAP</b>	0.015	2.503	0.0828 .
<b>UVA × Surfactants × Chla</b>	0.022	3.698	0.0272 *
<b>Date × Surfactants × NAP</b>	0.014	2.323	0.0980 .
<b>Date × Chla × NAP</b>	0.015	2.556	0.0774 .
<b>UVA × Chla × NAP</b>	0.046	7.896	0.0005 ***
<b>Surfactants × Chla × NAP</b>	0.019	3.162	0.0488 *
<b>Date × UVA × Surfactants × NAP</b>	0.022	3.675	0.0270 *
<b>Date × UVA × Chla × NAP</b>	0.017	2.958	0.0539 .
...			
<b>Residual</b>	0.147		



330 **Figure 6:** nMDS plot of the FDOM component composition depending on the layer (sea-surface microlayer (SML) and underlying water (ULW)) and bloom phase (onset, peak, decay). The SML is marked with triangles and the ULW is marked with circles. The phase of the phytoplankton bloom is indicated by different colors (orange: onset, light blue: peak, green: decay). The elliptic dotted line circle 75 % of points of each phase based on a multivariate normal distribution. The stress value (0.102) is displayed in the header and points to a good representation of the sample distance in the reduced ordination.

### 335 3.4 CDOM and FDOM time series results

While the PERMANOVA analyses focused on examining differences between the three bloom phases, this Sect. analyses temporal changes in CDOM and FDOM and the additional information CDOM/FDOM derived parameters deliver. The general trend of all CDOM/FDOM derived parameters either increased or decreased linearly during the study with some variations along the first bloom peak and with dependence on the sampling time (Figure 7, Figure 8, Table 5). While Figure 340 7 and Figure 8 shows the time series development of the FDOM components and four CDOM and FDOM derived parameters, Table 5 summarizes temporal dynamics and layer comparisons for all parameters mentioned in the methods Sect. 2. SML and ULW slopes and  $R^2$  were derived from linear correlations over the whole timeseries.  $\varnothing$  EF indicates the mean enrichment factor of the SML relative to the ULW over the whole study duration. “Layer Diff”, “Slope Diff”, and



“Variance Diff” in Table 5 denote the significance of differences between the respective means of the two layers, temporal  
345 trends (slopes), and variability, respectively, with significance indicated by asterisks (\*:  $p < 0.05$ ; \*\*:  $p < 0.01$ ; \*\*\*:  $p < 0.001$ ).

Figure 7 shows the time series results of the four PARAFAC components and their sum (Figure 7, first panel). Around the time of the first chlorophyll-a peak on May 28 a rise of the total fluorophores can be observed, driven by the rise of C3 in these samples. The PARAFAC fluorophore components followed different trends (Figure 7). The humic-like components  
350 (C1 and C2) declined, while the protein-like components (C3 and C4) increased. Fluorescence intensity was generally higher in the SML than in the ULW for all components except C4. Around the first chlorophyll-a peak from May 28-30, elevated values were observed for C1 and C3. All components apparently responded to the alternating morning and afternoon sampling, showing a “zig-zag” pattern in their temporal dynamics. However, the “zig-zag” pattern did not always follow the same direction. On some days, like May 19-23, the humic-like components had a higher intensity in the morning samples  
355 than in the previous afternoon samples in both the SML and ULW samples. On other days this pattern was reversed and differs between SML and ULW. C4 was the component with the largest relative differences in the general development during the mesocosm and in the daily changes.

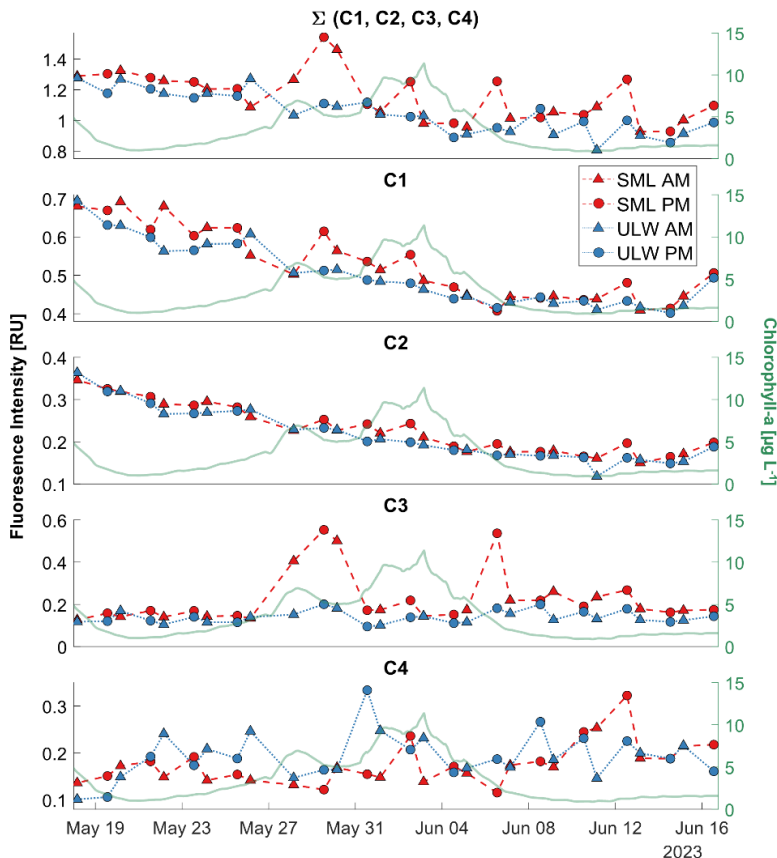


**Figure 7: Time series of fluorescent dissolved organic matter components (C1-C4) in Raman Units (RU) derived by PARAFAC analysis. The first panel shows the sum of all four components. Sea-surface microlayer samples are marked red, with a dashed line and the underlying water samples are marked blue with a dotted line. Morning samples (AM) are marked as triangles. Afternoon samples (PM) are marked with circles. On the right Y-axis the chlorophyll-a values in  $\mu\text{g L}^{-1}$  are drawn to help for an orientation within the development of the bloom during the mesocosm study.**

Figure 8 shows selected parameters listed in Table 5. The parameters not shown here exhibit similar trends to those displayed and are provided in the appendix (Figure A2). Figure 8 (left side) displays the time series of the parameters HIX, REPIX, SR, a254, and C1/a312, together with their first derivation (right side of Figure 8). The first derivation indicates the slope of the change from one timestep to the next one. If the value is above 0 it indicates a rise of the parameter towards that point in time, if it's lower than 0 it indicates a decrease. This emphasizes the differences between morning and afternoon sampling. These CDOM/FDOM derived parameters deliver information of the humification state (HIX, a254, C1/a312), photodegradation (HIX, SR, a254, C1/a312) and fresh production (REPIX).

The time series of the FDOM derived HIX showed a negative trend during the study. With the alternation of morning and afternoon sampling an irregular “zig-zag” pattern was observed (Figure 8a, b). The HIX values for SML and ULW samples of the morning and afternoon displayed different patterns throughout the study. From May 19-25, in the SML, the morning sample always had a higher HIX than the previous afternoon sample. For the ULW this pattern was reversed in this period.



375 In the middle of the study, during the phase of high chlorophyll-a, no specific pattern was observed. In the decaying phase of the bloom the pattern was the opposite to the first days specifically in the ULW. For the SML the trend changes a few times. The average EF is lower than 1, indicating a higher humification in the ULW (Table 5). In Figure 8b the beforementioned irregular “zig-zag” pattern was clearly observed as well. The HIX only had slightly significant differences between SML and ULW in the mean layer values, but no differences in the slope or the variance during the study.

380 Figure 8c and d show the time series and slope of the REPIX. REPIX increased in both the SML and the ULW. The values were enriched in the SML ( $\bar{\Omega}$  EF = 1.30). Around the time of the first bloom peak (May 28-30) and again for only one day after the second bloom (June 6) values in the SML are exceptionally high. Variance was significantly higher in the SML, and the layer mean values were differing significantly as well. For the slope of the REPIX (Figure 8d) no clear “zig-zag” pattern was observed for the morning and afternoon samples.

385 Panels e and f of Figure 8 show the time series and slope of the CDOM SR. The time series values of SML and ULW were both equally increasing during the study with almost constant and significantly higher values in the SML ( $\bar{\Omega}$  EF = 1.03). Figure 8f reveals that throughout the study the SR only decreases towards the morning samples in the SML and ULW but more often in the SML.

390 Shown in Figure 8 (g and h) are the time series of the absorption coefficient at 254 nm (g) and the slope between the samples (h). A significant difference in SML and ULW can be observed in the layer mean values of the absorption coefficient and the linear fit of the decline during the study (Table 5). A higher but not significant variability is visible for the SML ( $R^2 = 0.02$ ) than for the ULW ( $R^2 = 0.76$ ). From the a254 derivation in Figure 8h it's also visible that only the slope towards the SML morning samples is ever very low (< -1) indicating an overnight decrease in aromaticity in the SML.

395 Higher values at the beginning of the study in the C1/a312 ratio (Figure 8, i and j) suggested that the marine humic-like substances are more humified or less photodegraded. This ratio declines in both SML and ULW. The difference in the slope of the linear fit and the variance in SML and ULW was significant (both:  $p < 0.01$ , Table 5), the ratio declined faster in the SML. BIX (Figure A2a) and the C3/C1 ratio (Figure A2b) were both significantly higher in the SML than in the ULW throughout the study and had a similar time series development like the REPIX (Figure 8c).

400 **Table 5: Sea-surface microlayer (SML) and underlying water (ULW) linear trends (slope,  $R^2$ ) and mean enrichment factor ( $\bar{\Omega}$  EF) for dissolved organic matter parameters described in Table 1. Significance of differences between both layers as layer means, slopes, and variance are indicated in Layer Diff, Slope Diff, and Variance Diff (highly significant/ $p < 0.001$ : ‘\*\*\*’, significant/ $p < 0.01$ : ‘\*\*’, moderately significant/ $p < 0.05$ : ‘\*’, slightly significant/ $p < 0.1$ : ‘.’, not significant/ $p < 1$ : ‘ns’).**

Parameters	SML slope	SML $R^2$	ULW slope	ULW $R^2$	$\bar{\Omega}$ EF	Layer Diff	Slope Diff	Variance Diff
$\Sigma(C1, C2, C3, C4)$	-0.0111	0.39	-0.0128	0.74	1.11	***	ns	ns
C1	-0.0092	0.80	-0.0082	0.81	1.05	***	ns	ns
C2	-0.0060	0.87	-0.0064	0.86	1.07	***	ns	ns



<b>C3</b>	0.0013	0.01	0.0005	0.03	1.56	***	ns	*
<b>C4</b>	0.0028	0.30	0.0012	0.05	0.96	ns	ns	ns
<b>HIX</b>	-0.1180	0.63	-0.1190	0.60	0.93	.	ns	ns
<b>BIX</b>	0.0059	0.16	0.0071	0.63	1.06	**	ns	.
<b>REPIX</b>	0.0173	0.08	0.0130	0.36	1.30	***	ns	**
<b>C3/C1</b>	0.0086	0.09	0.0053	0.36	1.48	***	ns	**
<b>C1/a312</b>	-0.0009	0.66	-0.0005	0.48	0.99	ns	**	**
<b>SR</b>	0.0109	0.80	0.0108	0.95	1.03	***	ns	ns
<b>a254</b>	-0.0095	0.02	-0.0447	0.76	1.07	***	**	ns
<b>a440</b>	-0.0030	0.13	-0.0062	0.89	1.13	***	*	ns

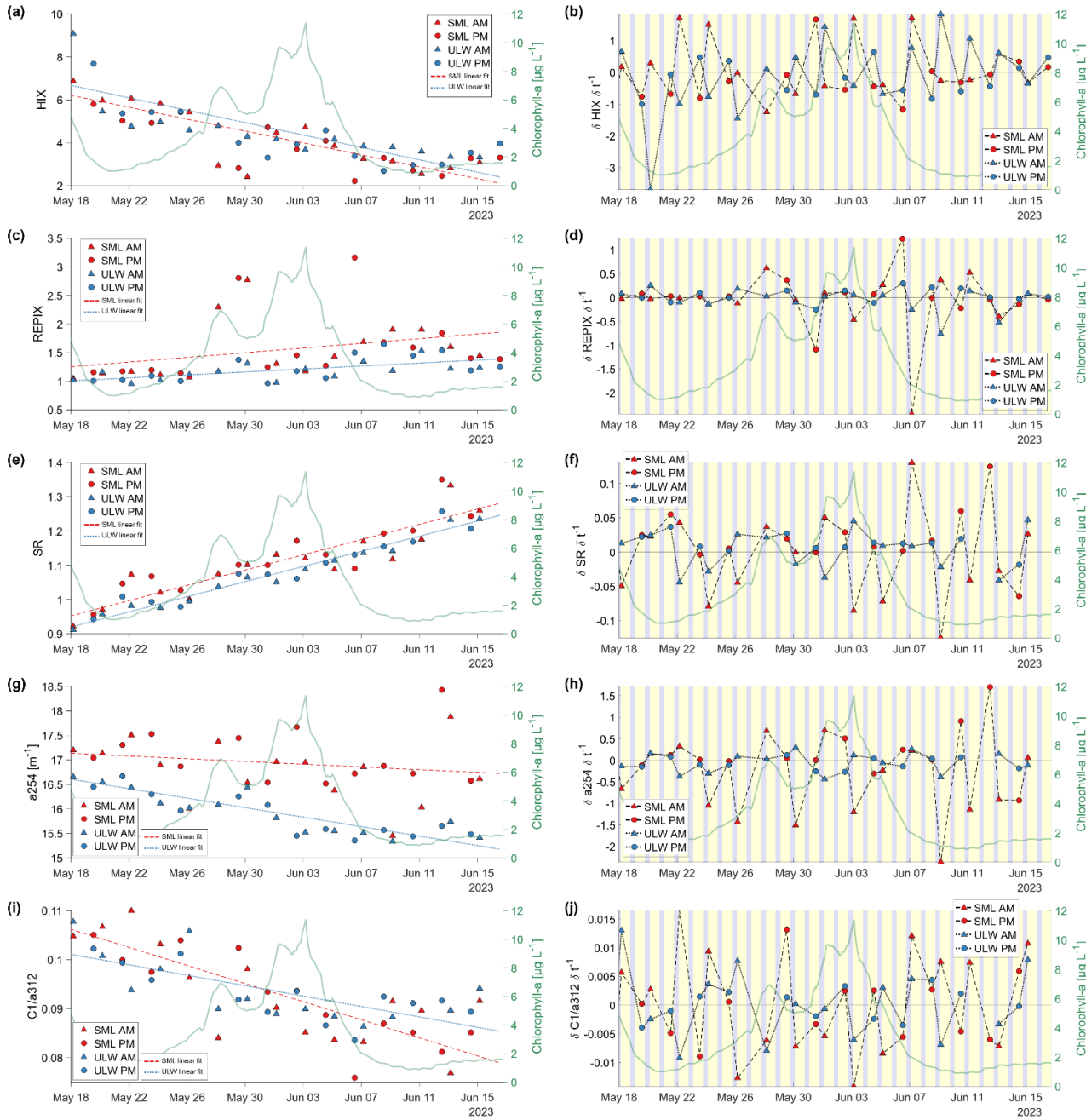


Figure 8: Left side: Time series results of the humification index (HIX, Zsolnay et al., 1999, a), the recently produced index (REPIX, Drozdowska et al., 2013, c) the slope ratio (SR, Helms et al., 2008, e), the absorption coefficient at 254 nm in  $\text{m}^{-1}$  (a254, Summers et al., 1987; Weishaar et al., 2003, g) and the ratio of PARAFAC component C1 and the absorption coefficient at 312 nm (C1/a312, DeHaan, 1993; Lønborg et al., 2010, i). The sea-surface microlayer (SML) samples are marked in red, with a dashed red linear fit line, and the underlying water (ULW) samples are marked in blue with a dotted blue linear fit line. Morning (AM) samples are marked with triangles, afternoon (PM) samples are marked with squares. Right side: The first derivation of HIX (b), REPIX (d), SR (f) and a254 (h). The background colors indicate the day (yellow) and night (grey) cycle. Right axes on both left and right side show the chlorophyll-a values in  $\mu\text{g L}^{-1}$ .



### 3.5 Correlations between SML and ULW, CDOM/FDOM derived parameters and environmental variables

415 The results of this Sect. 3.5 are displayed in the appendix. Figure A1 shows the correlation matrix, based on a Spearman correlation, for the FDOM components and the environmental variables in the SML (a) and the ULW (b), and for the CDOM/FDOM derived parameters and the environmental variables for the SML (c) and the ULW (d). The color bar displays the  $R^2$  value from 1 (red) to -1 (blue) and the white stars indicate the significance of the correlation (\*  $p < 0.05$ ; \*\*  $p < 0.01$ ; \*\*\*  $p < 0.001$ ). Only the significant correlations are displayed.

420 Figure A3 shows the relationship between the HIX and the integrated UVA irradiance in  $\text{W m}^{-2}$ , separated for SML in the morning (a), SML in the afternoon (b), ULW in the morning (c) and ULW in the afternoon (d). Within each plot  $R^2$ , Spearman's  $\rho$  and a linear correlation significance  $p$  are shown. None of the relationships have a significant correlation. But the afternoon sample data (Figure A3b, d) showed more pronounced negative relationships between the integrated UVA and the HIX than the morning samples.

425 While the previous analyses considered the SML and ULW separately, comparing their parameter dynamics, Figure A4 explores correlations between the layers to reveal their coupling or decoupling processes. The fluorophore intensities behaved differently in the SML and the ULW for single components (Figure A4, upper panel). The intensities for the marine humic-like C1 and humic-like component C2 were significantly linearly correlated between ULW and SML with high  $R^2 > 0.89$  ( $p < 0.001$ ). Between the protein-like components, the tryptophan-like component C3 was significantly correlated with 430 a smaller  $R^2$  ( $R^2 = 0.46$ ,  $p < 0.001$ ) while the component C4 was not correlated ( $R^2 = 0.04$ ,  $p = 0.292$ ) between ULW and SML. The same linear correlation between ULW and SML was drawn for two absorption coefficients (a254, a440), the SR and C1/a312 (Figure 7, lower panel). Both absorption coefficients were enriched in the SML, as they lay above the 1:1 line. While a254 was not correlated, a440 was significantly correlated between ULW and SML. The SR was higher in the SML and strongly correlated between ULW and SML. The C1/a312 ratio was also significantly correlated between ULW and 435 SML and higher in the SML.

## 4 Discussion

### 4.1 Hypothesis 1: CDOM and FDOM signatures in SML and ULW shaped by a phytoplankton bloom

Two overlapping phytoplankton blooms developed during the mesocosm study following nutrient additions on May 26, May 440 30, and June 1. The first, peaking on May 28, was dominated by *E. huxleyi*, and the second, on June 3, by *C. closterium* (Bibi et al., 2025a). Chlorophyll-a concentrations in the SML were distinctly higher ( $\text{OEF} = 49.75$ ) and more delayed than in the ULW (Figure 2a). Hardy and Apts (1984) and Antonowicz (2018) have reported an enrichment of chlorophyll-a in the SML but not at similar magnitudes as they have been measured here. Although independent chlorophyll production by phytoplankton has been reported (Hardy, 2009; Hardy and Apts, 1984; Obernosterer et al., 2005; Reinhäuser et al., 2008; Wurl et al., 2016), the strong enrichment observed here likely reflects passive accumulation rather than active growth. The SML



445 appeared dominated by brown detritus, and QFT-ICAM absorption spectra confirmed that elevated chlorophyll concentrations coincided with strong NAP absorption in the near-infrared (Figure 2a, b). This pattern suggested that detritus and phytoplankton cells accumulated in the SML through physical processes such as bubble transport (Hardy, 1982) or vertical mixing. Cooling of the SML at night, increased its density and promoted buoyancy fluxes, which may have further enhanced this exchange (Rauch et al., 2025).

450 Generally, the mesocosm bloom and the three bloom phases were defined by the chlorophyll-a concentration time series of the ULW and it was hypothesized that the CDOM and FDOM signatures in the SML and ULW provide information on the transformation processes of DOM and differ considerably between the two layers.

Phytoplankton exudation is typically associated with protein-like and marine humic-like FDOM (Chari et al., 2013; Romera-Castillo et al., 2010; Stedmon and Markager, 2005), suggesting a potential link between bloom progression and components 455 C1, C3, and C4. However, neither individual FDOM components nor the CDOM/FDOM derived parameters followed the chlorophyll-a trend in the ULW (Figure 2a, Figure 7, Figure A1). In contrast, several FDOM indices (C1, C2, and most CDOM/FDOM derived parameters except a254) correlated significantly with chlorophyll-a in the SML, though this relationship may in part reflect the concurrent progression of time (Figure A1).

PERMANOVA and nMDS analyses further support a strong temporal control on FDOM composition, with clear clustering 460 by bloom phase but not by layer (Table 3, Table 4, Figure 6). The absence of a significant phase-layer interaction ( $p = 0.2993$ ) indicated that bloom development and the layer affected FDOM independently. These results suggested that temporal drivers such as photodegradation and microbial processing, rather than chlorophyll-a dynamics alone, governed the observed FDOM composition in the mesocosm.

The time series of FDOM components revealed distinct differences between SML and ULW, mainly in their mean layer 465 values (Table 5). Throughout the study, humic-like material steadily decreased (Figure 5, Figure 7). While C2 declined linearly, C1 showed elevated SML values, peaking shortly after the *E. huxleyi* bloom (May 28-30). C1 fluorescence is linked to phytoplankton production (Chari et al., 2013; Coble et al., 1998) and microbial processing of algal DOM (Stedmon and Markager, 2005). The same three days also showed elevated C3, associated with tryptophan-like fluorescence from phytoplankton or microbes (Harris et al., 2024; Obernosterer et al., 2005; Rochelle-Newall et al., 2004; Romera-Castillo et 470 al., 2010). Bacterial abundance data from Bibi et al. (2025a) confirm higher SML values on May 28, the first day of increased C1 and C3 (Figure 2d). Despite low temporal resolution, these results suggest a microbial contribution to FDOM. Passive accumulation of OM in the SML suggested that detritus and its microbial degradation represented key CDOM and FDOM sources. Zöbelein et al. (in prep.), who analyzed DOM composition at the molecular level during the same mesocosm study, similarly observed carbohydrate-rich DOM accumulation in the SML after the bloom, likely from phytoplankton 475 exudation, particle degradation, and microbial transformation. In a different mesocosm study, Rochelle-Newall et al. (2004) found no link between CDOM absorption and *E. huxleyi* abundance, attributing this to minimal differences in metabolic activity or DOM composition. However, Retelletti Brogi et al. (2020) associated *E. huxleyi* exudates with fluorescence in the C3 and C1 regions, with tryptophan-like components (C3) dominating. Similarly, Romera-Castillo et al. (2010) showed that



phytoplankton species, nutrients, and light affect FDOM quality, reflected in the C3/C1 ratio. In our study, elevated C3/C1  
480 ratios (Figure A2b), BIX (Figure A2a), and REPIX (Figure 8c) in the SML during the bloom peak (Figure A2b) further support these findings.

While previous studies have reported significant enrichment of protein-like fluorescence in the SML (Blough, 1997; Galgani and Engel, 2016; Yang et al., 2022), the mesocosm results showed enhanced C1 and C3 enrichment only during the *E. huxleyi* bloom peak. Nevertheless, enrichment factors for all components except C4 exceeded one (Table 5). Galgani and

485 Engel (2016) attributed protein-like enrichment to microbial sources within the SML or immediate subsurface, while humic-like material likely originated from the ULW and was transported upward by physical processes, an interpretation that may also apply in our study. Yang et al. (2022) observed strong correlations of CDOM and FDOM between the SML and subsurface water, indicating vertical coupling and DOM exchange. Similar correlations were found for most mesocosm parameters (Figure A4), except for C4 and a254. In their study, tyrosine-like fluorescence increased under photochemical

490 exposure while humic-like components decreased, suggesting transformation of aromatic DOM into protein-like material.

Our C4 showed no correlation between SML and ULW, implying independent transformation pathways in both layers (Figure A4, C4). During the *E. huxleyi* bloom, C3 was enriched in the SML, whereas C4 remained similar or higher in the ULW. The lack of coupling suggests that unlike in Yang et al. (2022), tyrosine-like FDOM production in the mesocosm was controlled by local microbial or photochemical processes rather than vertical exchange, indicating layer-specific cycling  
495 under bloom conditions. During the subsequent *C. closterium* bloom (May 31-June 4), only a slight increase of C4 was detected in the ULW (Figure 7). Although Chari et al. (2013) demonstrated that *C. closterium* releases protein-like, humic-like, and marine humic-like FDOM even in bacteria-free cultures, no clear link between this diatom bloom and the observed fluorophores emerged in our study.

The irregular fluctuations of CDOM/FDOM derived parameters between sampling events further suggested dynamic  
500 transformation, production and exchange processes between the SML and the ULW rather than a steady photodegradation trend, see Sect. 4.2 (Figure 7, Figure 8). If photochemical loss of humic-like material were dominant, afternoon samples would have shown a relative increase in protein-like fluorescence; instead, DOM intensities exhibited a “zig-zag” pattern, indicating that multiple sinks and sources of DOM, possibly with diurnal variability, operated simultaneously. Phytoplankton exudation of DOM likely contributed to these patterns. During daylight, exudation of labile, low-molecular-weight  
505 compounds associated with protein-like FDOM (tryptophan- and tyrosine-like fluorescence) was enhanced, whereas nighttime processes favor the release of polymeric carbohydrates and the accumulation of humic-like FDOM (Kieber et al., 1989; Smith and Underwood, 2000; Stedmon and Markager, 2005; Thornton, 2014). Consequently, daytime conditions favored the accumulation of freshly produced, protein-like DOM, whereas nighttime processes promote its transformation into more humified, refractory compounds. Indices reflecting microbial alteration, such as BIX and REPIX, further  
510 supported a shift toward freshly produced DOM. BIX values rose from ~0.8 to ~1 during the study (Figure A2a), indicating increasing bacterial influence consistent with rising bacterial abundance (Bibi et al., 2025a).



While the bloom phases influenced the general DOM composition, most observed changes appeared to result from passive accumulation, microbial transformation, and photochemical processes rather than direct phytoplankton exudation. Yet clear differences in the mean layer values for most CDOM/FDOM derived parameters and subtle responses of the C3/C1, BIX and 515 REPIX to the *E. huxleyi* bloom indicate connections of the phytoplankton bloom to the bio-optical proxies. Therefore, these data partly support the hypothesis that the CDOM and FDOM signatures in the SML and ULW provide information on the transformation processes of DOM and differ considerably between the two layers.

#### 4.2 Hypothesis 2: Photodegradation of CDOM and FDOM in the SML vs. in the ULW

The SML's strong exposure to solar radiation and UV degradation is considered a key factor shaping its distinct physical and 520 chemical properties (Blough, 1997; Cunliffe et al., 2013; Drozdowska et al., 2017; Galgani and Engel, 2016). Accordingly, it was hypothesized that photodegradation during the mesocosm study affects the DOM in the SML more than in the ULW, especially regarding the production of OM during the phytoplankton blooms. Previous field studies have shown stronger photochemical impacts on the SML compared to the ULW, sampled at depth  $\geq 1$  m (Drozdowska et al., 2017; Miranda et al., 2018; Yang et al., 2022) and in about 0.2 m depth (Galgani and Engel, 2016). During the mesocosm study (total depth of 0.8 525 m), the ULW was sampled at 0.4 m to resolve near-surface effects. Alternating morning-afternoon sampling was conducted to capture diel exposure differences ( $\sim 1$  h vs.  $\sim 10$  h of sunlight).

Aromatic molecules are preferentially degraded by UV exposure compared to amide- and peptide-like carbons (Helms et al., 530 2014; Stedmon and Markager, 2005). Photodegradation breaks down conjugated aromatic structures, producing smaller, less conjugated molecules that absorb predominantly in the UV region, thus increasing the CDOM spectral slope (Helms et al., 2008; Moran and Zepp, 1997). Therefore, a rise in the SR is expected as a sign of photodegradation. While photodegradation increases the SR, microbial alteration of CDOM decreases the SR over timescales of days to weeks (Galgani and Engel, 2016; Helms et al., 2008). CDOM/FDOM derived parameters delivering information of the humification state (HIX, a254, C1/a312), are expected to decrease by photodegradation.

In the mesocosm study, the SR in SML and ULW increased almost linearly, while mean SR values were slightly higher in 535 the SML (Figure 8e, Table 5), indicating a marginally stronger effect near the surface. However, other indicators showed contrasting trends: a254 declined more slowly in the SML, suggesting greater aromatic content, while C1/a312 decreased faster, implying enhanced degradation. These inconsistencies point to overlapping processes influencing DOM composition in both layers.

As mentioned in the previous Sect. 4.1, CDOM and FDOM dynamics in the SML and ULW showed irregular, “zig-zag” 540 patterns rather than a steady photodegradation trend, reflecting simultaneous photochemical, microbial, and phytoplankton-driven processes. Daytime favored production of protein-like, labile DOM, while nighttime promoted its transformation into humic-like, more refractory compounds. Microbial alteration, indicated by rising BIX values, also contributed to the accumulation of freshly produced DOM. The SR continuously increased in both layers (SML fit = 0.0109; ULW = 0.0108), suggesting that photodegradation outweighed microbial alteration as a sink. Declining HIX values supported the progressive



545 degradation of aromatic material and corresponded with the observed decrease in humic-like components (C1, C2) and  
increase in protein-like ones (C3, C4) during the study (Figure 7, Table 5). No significant correlation was found between  
HIX and daily irradiance (Figure A3), yet afternoon samples tended to show a lower HIX under stronger light exposure,  
consistent with photodegradation effects on aromatic material. Similar trends have been reported by Miranda et al. (2018),  
Yang et al. (2022), and Drozdowska et al. (2017), who observed reduced humic-like fluorescence and higher SR values in  
550 the SML due to the photochemical breakdown of aromatic DOM.

The initially high C1 and C2 intensities likely reflected the influence of riverine and sediment-derived DOM in Jade Bay  
source water (van Beusekom et al., 2012; Liebezeit et al., 1994). The concurrent decline of humic-like and increase of  
protein-like fluorescence supported a gradual shift from terrestrial and refractory DOM toward fresher, biologically and  
photochemically altered material during the mesocosm study.

555 At the molecular level, Zöbelein et al. (in prep.) observed similar trends in the same mesocosm study, showing a decline in  
aromatic molecules towards the end of the study. They found no major compositional differences between SML and ULW,  
suggesting that strong vertical coupling and high light penetration promoted uniform photodegradation across layers. Jibaja  
Valderrama et al. (2025) detected enhanced photochemical activity in the SML, with elevated production of low-molecular-  
weight carbonyl compounds under high biological productivity, though the total light-induced formation of  
560 oxidants remained similar in both layers. Their results indicate that while the SML acts as a hotspot for reactive  
photoproducts, the overall photooxidation capacity is comparable in both layers.

Next to the phytoplankton-derived DOM, atmospheric deposition may have contributed as a source of DOM (Galletti et al.,  
2020; Hunter, 1980) and should be considered for future studies. Since the roof of SURF was closed during rain events and  
565 at night, most atmospheric depositions probably occurred during the day, and wet depositions can be excluded. Another  
possible sink of DOM to be considered is the aggregation of high molecular weight components into gel particles, a physical  
process that transfers dissolved molecules into the particulate size spectrum and increases the chance of physical sinking of  
the particles (Engel et al., 2011; Verdugo, 2012).

While photodegradation clearly acted as a major sink for aromatic DOM during the mesocosm study, its effects were  
comparable in the SML and ULW. The expected stronger degradation in the SML was not observed conclusively, likely due  
570 to the multiple overlying transformation processes, the shallow basin, strong vertical mixing, and uniform light penetration  
preventing pronounced gradients. Therefore, the initial hypothesis that photodegradation would more strongly affect the  
SML than the ULW was not supported under the given conditions, though it may apply in more stratified natural systems  
where vertical gradients in light and DOM composition are stronger.

## 5 Conclusion

575 In this mesocosm study, the influence of an induced phytoplankton bloom and photodegradation on CDOM and FDOM  
dynamics in the SML and the ULW were investigated. Daily SML and ULW samples were taken alternatively ~1 h and



~10 h after sunrise and analyzed for their absorption and fluorescence properties. These can deliver insights into DOM transformation processes, such as production, transport, and degradation. The SML has distinct physical and chemical features compared to the ULW. If it is enriched in DOM, it can hinder exchange processes between the ocean and the  
580 atmosphere. Temporal dynamics of the processes leading to an enrichment of DOM in the SML are insufficiently understood. It was hypothesized that the CDOM and FDOM signatures in the SML and ULW provide information on the transformation processes of DOM and differ considerably between the two layers and that photodegradation during the mesocosm study affects the DOM in the SML more than in the ULW, especially regarding the production of OM during the phytoplankton blooms.

585 The mesocosm study showed that phytoplankton bloom dynamics only partially shaped CDOM and FDOM signatures in the SML and ULW. While different bloom phases influenced the general DOM composition, most observed changes appeared to result from passive accumulation, microbial transformation, and photochemical processes rather than direct phytoplankton exudation. Photodegradation emerged as a major sink for aromatic DOM, but its effects were similar in both the SML and  
590 ULW, likely due to strong vertical mixing, shallow water depth, and high light penetration, which prevented the formation of surface-specific photochemical gradients.

One shortcoming of the described mesocosm setup was the limited daily sample volume, to maintain the integrity of the SML which led to a lack of statistical significance, since there were no replicates possible. Furthermore, future studies could benefit from using artificial seawater with a small inoculum of natural phytoplankton, which would reduce background DOM that might otherwise mask DOM transformation effects.

595 Our findings highlight that SML specific processes may be subtle and that even higher temporal and vertical resolution sampling, combined with interdisciplinary collaboration, will be essential to better distinguish between possible sinks and sources of DOM in future studies.



## Appendix

600

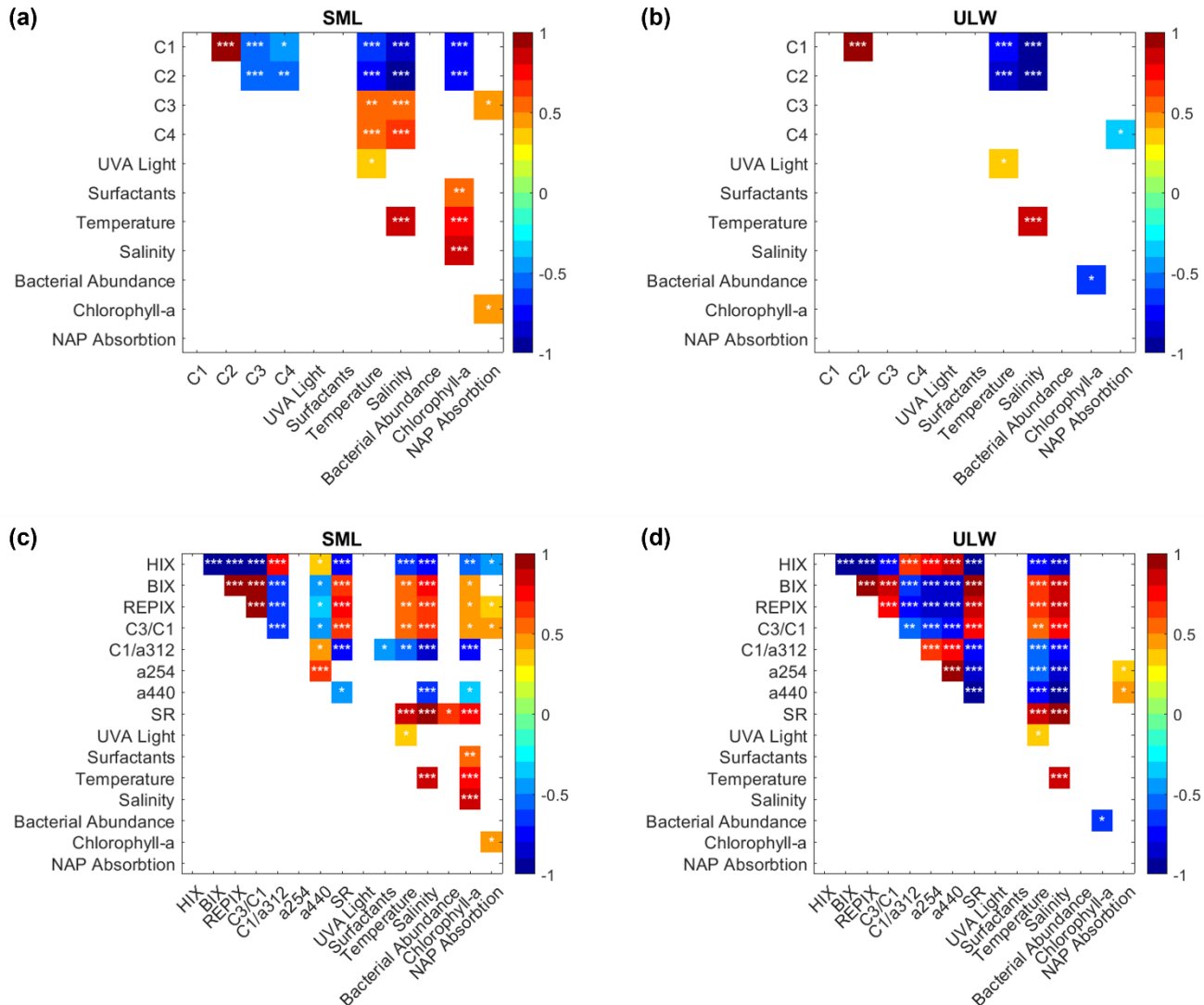
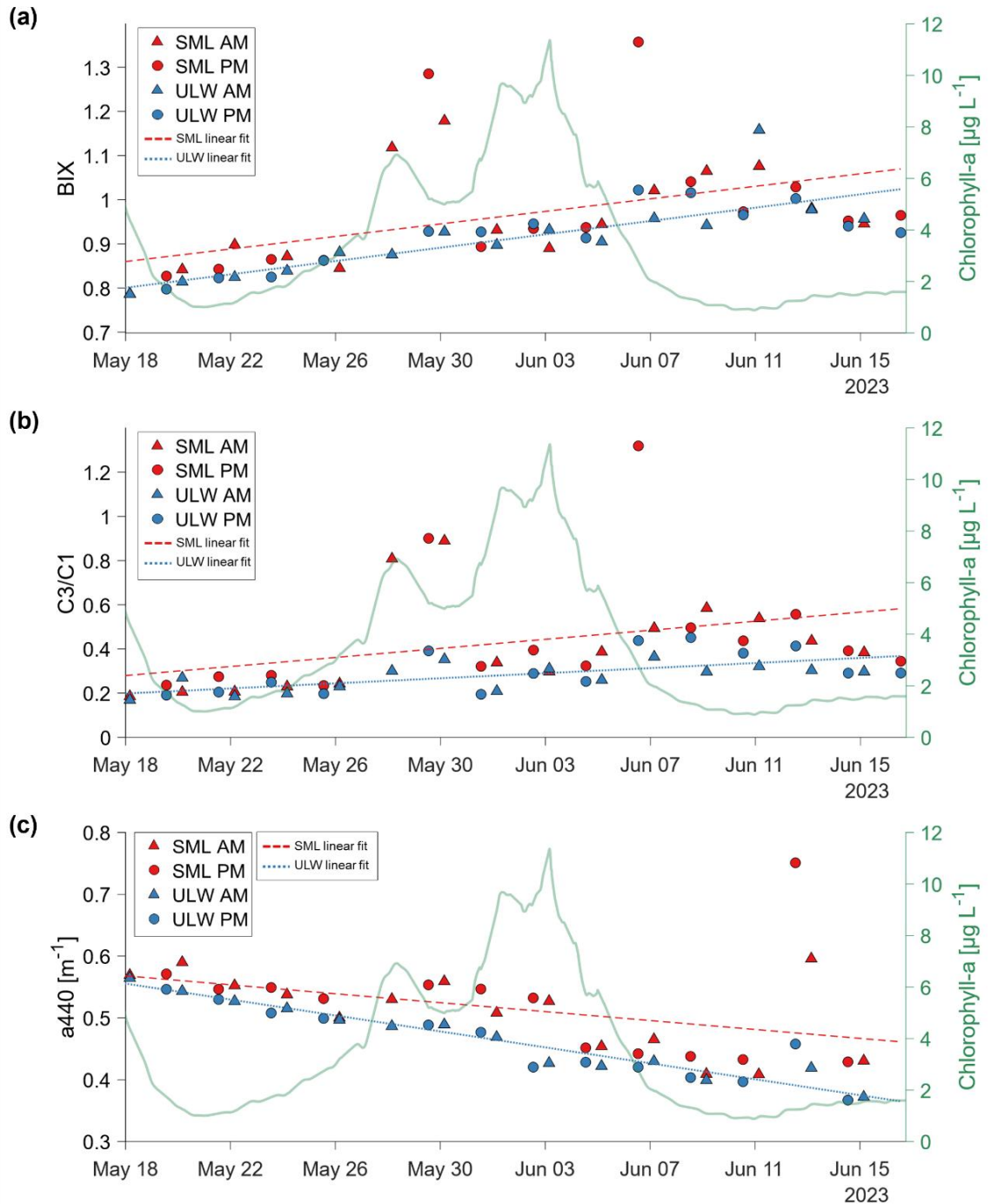
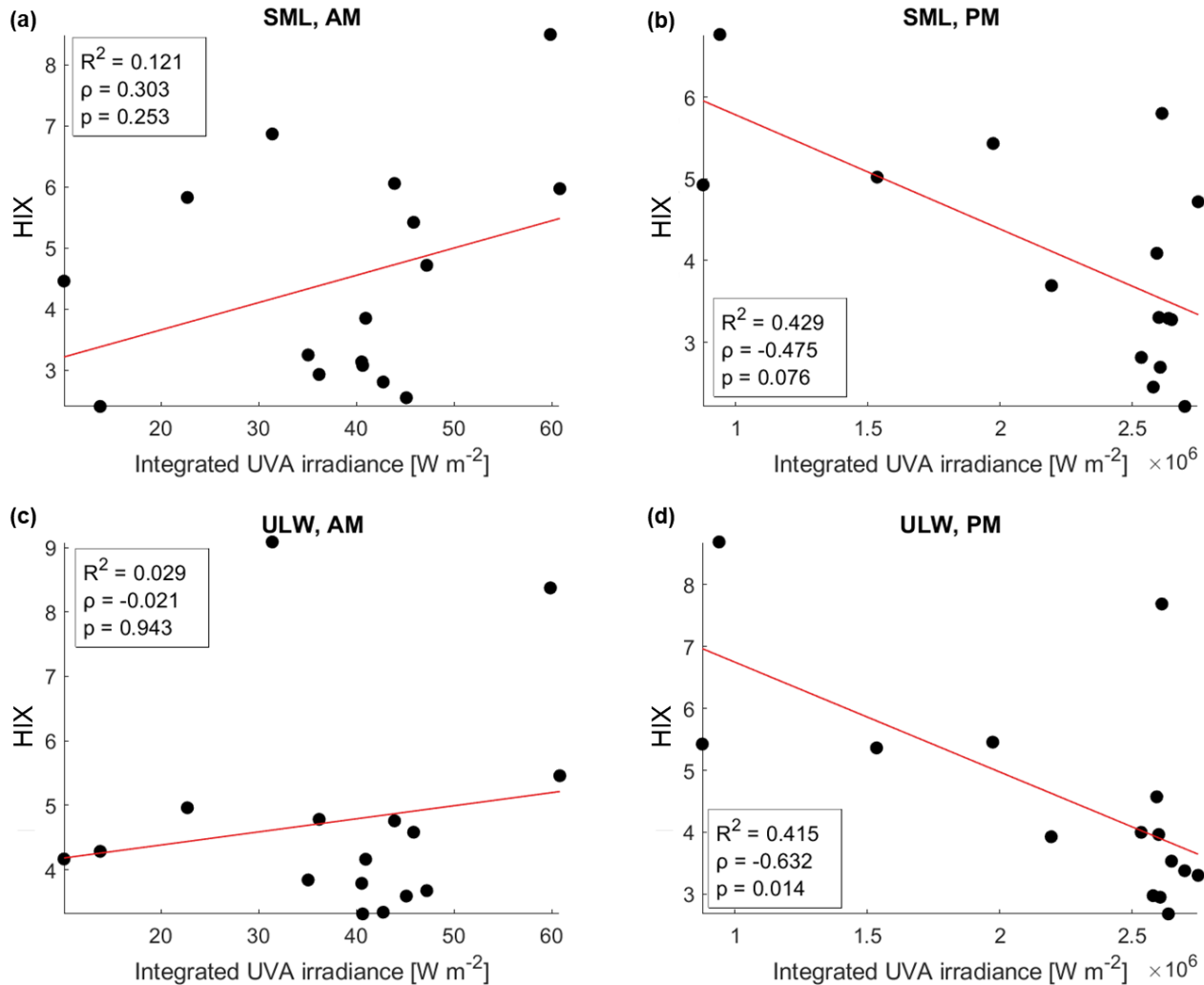


Figure A1: Spearman correlations matrix of FDOM components and environmental variables (Sea-surface microlayer (SML): a, Underlying water (ULW): b) and CDOM/FDOM derived parameters and environmental variables (SML: c, ULW: d). Only the significant correlations are shown ( $p < 0.5$ ). The asterisks in the cells indicate the level of significance (\*  $p < 0.05$ ; \*\*  $p < 0.01$ ; \*\*\*  $p < 0.001$ ). The color indicates the level of  $R^2$  where red means positively correlated and blue means negatively correlated. The abbreviations used in the figure are explained in Table 1.

605



**Figure A2:** Time-series results of the (a) biological index (BIX, Huguet et al., 2009), (b) the ratio of PARAFAC component C3 and C1 (Romera-Castillo et al., 2010), and (c) the absorption coefficient at 440 nm in m<sup>-1</sup> (a440). The sea-surface microlayer (SML) samples are marked in red, with a dashed red linear fit line, and the underlying water (ULW) samples are marked in blue with a dotted blue linear fit line. Morning (AM) samples are marked with triangles, afternoon (PM) samples are marked with squares. Right axes show the chlorophyll-a values in µg L<sup>-1</sup>.



**Figure A3: Integrated UVA irradiance vs. the humification index (HIX, Zsolnay et al., 1999) for the sea-surface microlayer (SML) morning (AM) (a) and afternoon (PM) (b) samples and the underlying water (ULW) AM (c) and PM (d) samples.**

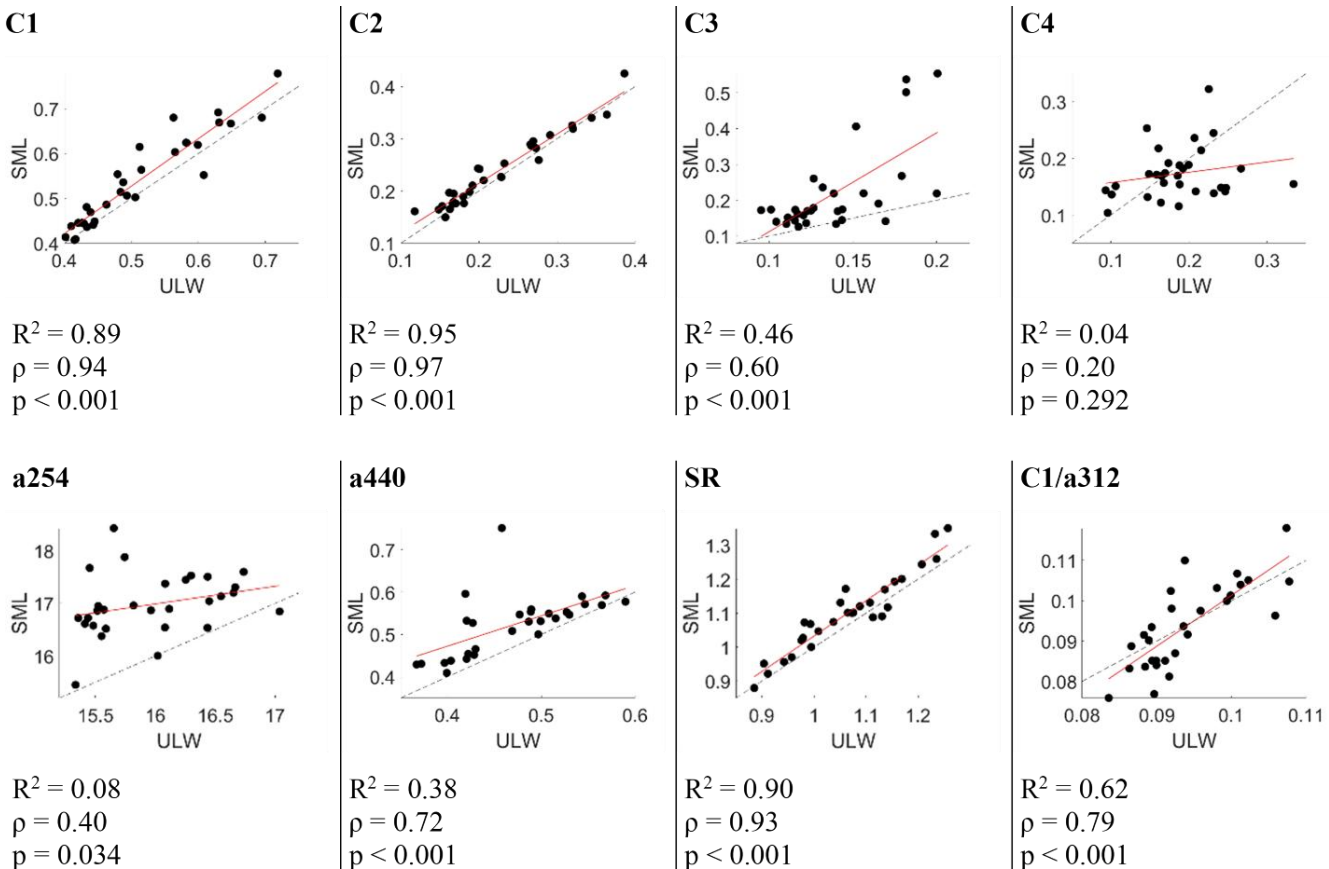


**Figure A4: Linear correlation between the underlying water (ULW) and the sea-surface microlayer (SML) for FDOM fluorophore intensities C1-C4 in Raman units (RU), two absorption coefficients (a254, a440), the slope ratio (SR) and the ratio of C1 and the absorption coefficient at 312 nm (C1/a312). The dotted line indicates the 1:1 line and the red line is the linear fit. The coefficient of determination ( $R^2$ ), Spearman's  $\rho$  and its significance are noted underneath each plot.**

620

**Data availability.** CDOM and FDOM data have been submitted to PANGAEA and are currently awaiting DOI assignment. Data from discrete samples during the mesocosm study, like chlorophyll-a, surfactants, and overall bacterial abundance, are available at PANGEA in Bibi et al. (2025b). All data are available on request from the corresponding author.

625

#### Author contributions

CT: Data Curation, Formal Analysis, Methodology, Visualization, Writing – Original Draft, Writing – Review & Editing,  
 JW: Conceptualization, Data Curation, Formal Analysis, Supervision, Writing – review and editing,  
 MGN: Data Curation, Formal Analysis, Writing – Review & Editing,  
 RR: Funding Acquisition, Conceptualization, Data Curation, Formal Analysis, Supervision, Writing – Review & Editing,  
 OZ: Funding Acquisition, Conceptualization, Supervision, Writing – Review & Editing.



**Competing interests.** The authors declare that they have no conflict of interest.

635 **Acknowledgements.** The authors would like to thank all members of the BASS research group and the ICBM workshop for the successful teamwork and their help conducting the SURF mesocosm study in 2023. We acknowledge Oliver Wurl and Riaz Bibi for their coordination and organization of the BASS mesocosm study. We are grateful to our colleagues Kai Schwaltenberg for helping with PARAFAC, Oliver Ferdinand for providing his bottle preparation protocol for the fluorometric analysis and Kerstin Heymann for conducting the HPLC analysis. We thank Isha Athale, Dmytro Spriahailo, 640 Thorsten Brinkhoff, Thomas Reinthaler from BASS SP1.2 for providing the bacterial abundance data. We thank Carsten Rauch and Oliver Wurl from BASS SP2.3 for providing additional CTD data. ChatGPT (OpenAI, 2025) was used for text refinement and language polishing.

645 **Funding.** This research was supported by the project “Biogeochemical processes and Air–sea exchange in the Sea-Surface microlayer (BASS)”, which was funded by the German Research Foundation (DFG) under Grant No 451574234.

## References

Álvarez-Salgado, X. A., Nieto-Cid, M., and Rossel, P. E.: Dissolved Organic Matter, in: Marine Analytical Chemistry, edited by: Blasco, J. and Tovar-Sánchez, A., Springer Nature, Switzerland, 2023.

Anderson, M. J.: A new method for non-parametric multivariate analysis of variance, *Austral Ecology*, 26, 32–46, 650 <https://doi.org/10.1111/j.1442-9993.2001.01070.pp.x>, 2001.

Antonowicz, J. P.: Air-Water Interface in an Estuarine Lake: Chlorophyll and Nutrient Enrichment, *Polish Journal of Ecology*, 66, 205, <https://doi.org/10.3161/15052249PJE2018.66.3.001>, 2018.

Baker, A., Bolton, L., Newson, M., and Spencer, R. G. M.: Spectrophotometric properties of surface water dissolved organic matter in an afforested upland peat catchment, *Hydrological Processes*, 22, 2325–2336, <https://doi.org/10.1002/hyp.6827>, 655 2007.

Balch, W. M.: The Ecology, Biogeochemistry, and Optical Properties of Coccolithophores, *Ann Rev Mar Sci*, 10, 71–98, <https://doi.org/10.1146/annurev-marine-121916-063319>, 2018.

Barthelmeß, T. and Engel, A.: How biogenic polymers control surfactant dynamics in the surface microlayer: insights from a coastal Baltic Sea study, *Biogeosciences*, 19, 4965–4992, <https://doi.org/10.5194/bg-19-4965-2022>, 2022.

660 van Beusekom, J. E. E., Buschbaum, C., and Reise, K.: Wadden Sea tidal basins and the mediating role of the North Sea in ecological processes: scaling up of management?, *Ocean & Coastal Management*, 68, 69–78, <https://doi.org/10.1016/j.ocecoaman.2012.05.002>, 2012.



Bibi, R., Ribas-Ribas, M., Jaeger, L., Lehnert, C., Gassen, L., Cortés, E., Wollschläger, J., Thölen, C., Waska, H., Zöbelein, J., Brinkhoff, T., Athale, I., Röttgers, R., Novak, M., Engel, A., Barthelmeß, T., Karnatz, J., Reinthaler, T., Spriahailo, D.,  
665 Friedrichs, G., Schäfer, F., and Wurl, O.: Biogeochemical Dynamics of the Sea-Surface Microlayer in a Multidisciplinary Mesocosm Study, EGUsphere, <https://doi.org/10.5194/egusphere-2025-1773>, 2025a.

Bibi, R., Ribas-Ribas, M., Jaeger, L., Lehnert, C., Gassen, L., Cortés, E., Wollschläger, J., Thölen, C., Waska, H., Zöbelein, J., Brinkhoff, T., Athale, I., Röttgers, R., Novak, M., Engel, A., Barthelmeß, T., Karnatz, J., Reinthaler, T., Spriahailo, D., Friedrichs, G., Schäfer, F., and Wurl, O.: Physical, chemical, and biogeochemical parameters from a mesocosm experiment  
670 at the Sea Surface Facility (SURF), Wilhelmshaven, Germany, spring 2023, <https://doi.org/10.1594/PANGAEA.984101>, 2025b.

Blough, N. V.: Photochemistry in the sea-surface microlayer, in: The Sea Surface and Global Change, edited by: Liss, P. S. and Duce, R. A., Cambridge University Press, 383–424, <https://doi.org/10.1017/CBO9780511525025.014>, 1997.

Bricaud, A., Morel, A., and Prieur, L.: Absorption by dissolved organic matter of the sea (yellow substance) in the UV and  
675 visible domains, *Limnology & Oceanography*, 26, 43–53, <https://doi.org/10.4319/lo.1981.26.1.0043>, 1981.

Brown, M. B. and Forsythe, A. B.: Robust Tests for the Equality of Variances, *Journal of the American Statistical Association*, 69, 364–367, 1974.

Calderó-Pascual, M., Yıldız, D., Yalçın, G., Metin, M., Yetim, S., Fiorentin, C., Andersen, M. R., Jennings, E., Jeppesen, E., Ger, K. A., Beklioğlu, M., and McCarthy, V.: The importance of allochthonous organic matter quality when investigating  
680 pulse disturbance events in freshwater lakes: a mesocosm experiment, *Hydrobiologia*, 849, 3905–3929, <https://doi.org/10.1007/s10750-021-04757-w>, 2022.

Carlucci, A. F., Craven, D. B., and Henrichs, S. M.: Surface-film microheterotrophs: amino acid metabolism and solar radiation effects on their activities, *Marine Biology*, 85, 13–22, 1985.

Catalá, T. S., Reche, I., Fuentes-Lema, A., Romera-Castillo, C., Nieto-Cid, M., Ortega-Retuerta, E., Calvo, E., Álvarez, M.,  
685 Marrasé, C., Stedmon, C. A., and Álvarez-Salgado, X. A.: Turnover time of fluorescent dissolved organic matter in the dark global ocean, *Nat Commun*, 6, 5986, <https://doi.org/10.1038/ncomms6986>, 2015.

Chari, N. V. H. K., Keerthi, S., Sarma, N. S., Pandi, S. R., Chiranjeevulu, G., Kiran, R., and Koduru, U.: Fluorescence and absorption characteristics of dissolved organic matter excreted by phytoplankton species of western Bay of Bengal under axenic laboratory condition, *Journal of Experimental Marine Biology and Ecology*, 445, 148–155,  
690 <https://doi.org/10.1016/j.jembe.2013.03.015>, 2013.

Chen, M., Jung, J., Lee, Y. K., and Hur, J.: Surface accumulation of low molecular weight dissolved organic matter in surface waters and horizontal off-shelf spreading of nutrients and humic-like fluorescence in the Chukchi Sea of the Arctic Ocean, *Science of The Total Environment*, 639, 624–632, <https://doi.org/10.1016/j.scitotenv.2018.05.205>, 2018.

Chen, S., Du, Y., Das, P., Lamore, A. F., Dimova, N. T., Elliott, M., Broadbent, E. N., Roebuck, J. A., Jaffé, R., and Lu, Y.:  
695 Agricultural land use changes stream dissolved organic matter via altering soil inputs to streams, *Science of The Total Environment*, 796, 148968, <https://doi.org/10.1016/j.scitotenv.2021.148968>, 2021.



Clarke, K. R.: Non-parametric multivariate analyses of changes in community structure, *Australian Journal of Ecology*, 18, 117–143, <https://doi.org/10.1111/j.1442-9993.1993.tb00438.x>, 1993.

700 Coble, P. G.: Characterization of marine and terrestrial DOM in seawater using excitation-emission matrix spectroscopy, *Marine Chemistry*, 51, 325–346, [https://doi.org/10.1016/0304-4203\(95\)00062-3](https://doi.org/10.1016/0304-4203(95)00062-3), 1996.

Coble, P. G.: Marine Optical Biogeochemistry: The Chemistry of Ocean Color, *American Chemical Society*, 38, 402–418, <https://doi.org/10.1002/chin.200720265>, 2007.

Coble, P. G.: Colored dissolved organic matter in seawater, in: *Subsea Optics and Imaging*, edited by: Watson, J. and Zielinski, O., Woodhead Publishing, Cambridge, 98–118, <https://doi.org/10.1533/9780857093523.2.98>, 2013.

705 Coble, P. G., Del Castillo, C. E., and Avril, B.: Distribution and optical properties of CDOM in the Arabian Sea during the 1995 Southwest Monsoon, *Deep Sea Research Part II: Topical Studies in Oceanography*, 45, 2195–2223, [https://doi.org/10.1016/S0967-0645\(98\)00068-X](https://doi.org/10.1016/S0967-0645(98)00068-X), 1998.

Coulson, L. E., Weigelhofer, G., Gill, S., Hein, T., Griebler, C., and Schelker, J.: Small rain events during drought alter sediment dissolved organic carbon leaching and respiration in intermittent stream sediments, *Biogeochemistry*, 159, 159–710 178, <https://doi.org/10.1007/s10533-022-00919-7>, 2022.

Cunliffe, M. and Wurl, O. (Eds.): Guide to best practices to study the ocean's surface, International Council for Science, Scientific Committee on Oceanic Research (SCOR), 118 pp., 2014.

715 Cunliffe, M., Engel, A., Frka, S., Gašparović, B., Guitart, C., Murrell, J. C., Salter, M., Stolle, C., Upstill-Goddard, R. C., and Wurl, O.: Sea surface microlayers: A unified physicochemical and biological perspective of the air–ocean interface, *Progress in Oceanography*, 109, 104–116, <https://doi.org/10.1016/j.pocean.2012.08.004>, 2013.

DeHaan, H.: Solar UV-light penetration and photodegradation of humic substances in peaty lake water, *Limnol. Oceanogr.*, 38, 1072–1076, 1993.

Dittmar, T. and Stubbins, A.: Dissolved Organic Matter in Aquatic Systems, in: *Treatise on Geochemistry*, edited by: Holland, H. D. and Turekian, K. K., Elsevier, 125–156, <https://doi.org/10.1016/B978-0-08-095975-7.01010-X>, 2014.

720 Drozdowska, V., Freda, W., Baszanowska, E., Rudź, K., Darecki, M., Heldt, J. R., and Toczek, H.: Spectral properties of natural and oil polluted Baltic seawater — results of measurements and modelling, *Eur. Phys. J. Spec. Top.*, 222, 2157–2170, <https://doi.org/10.1140/epjst/e2013-01992-x>, 2013.

Drozdowska, V., Wrobel, I., Markuszewski, P., Makuch, P., Raczkowska, A., and Kowalcuk, P.: Study on organic matter fractions in the surface microlayer in the Baltic Sea by spectrophotometric and spectrofluorometric methods, *Ocean Sci.*, 13, 725 633–647, <https://doi.org/10.5194/os-13-633-2017>, 2017.

Eder, A., Weigelhofer, G., Pucher, M., Tiefenbacher, A., Strauss, P., Brandl, M., and Blöschl, G.: Pathways and composition of dissolved organic carbon in a small agricultural catchment during base flow conditions, *Ecohydrology & Hydrobiology*, 22, 96–112, <https://doi.org/10.1016/j.ecohyd.2021.07.012>, 2022.

Efron, B.: *Bootstrap Methods: Another Look at the Jackknife*, in: *Breakthroughs in Statistics*, edited by: Kotz, S., Springer-730 Verlag New York, 1979.



Engel, A., Handel, N., Wohlers, J., Lunau, M., Grossart, H.-P., Sommer, U., and Riebesell, U.: Effects of sea surface warming on the production and composition of dissolved organic matter during phytoplankton blooms: results from a mesocosm study, *J Plankton Res.*, 33, 357–372, <https://doi.org/10.1093/plankt/fbq122>, 2011.

Engel, A., Bange, H. W., Cunliffe, M., Burrows, S. M., Friedrichs, G., Galgani, L., Herrmann, H., Hertkorn, N., Johnson, M., Liss, P. S., Quinn, P. K., Schartau, M., Soloviev, A., Stolle, C., Upstill-Goddard, R. C., van Pinxteren, M., and Zäncker, B.: The Ocean's Vital Skin: Toward an Integrated Understanding of the Sea Surface Microlayer, *Front. Mar. Sci.*, 4, <https://doi.org/10.3389/fmars.2017.00165>, 2017.

Frew, N. M., Nelson, R. K., Mcgillis, W. R., Edson, J. B., Bock, E. J., and Hara, T.: Spatial Variations in Surface Microlayer Surfactants and their Role in Modulating Air-Sea Exchange, *Gas Transfer at Water Surfaces*, 127, 153–159, <https://doi.org/10.1029/GM127p0153>, 2002.

Gade, M., Byfield, V., Ermakov, S., Lavrova, O., and Mitnik, L.: Slicks as Indicators for Marine Processes, *oceanog.*, 26, <https://doi.org/10.5670/oceanog.2013.39>, 2013.

Galgani, L. and Engel, A.: Changes in optical characteristics of surface microlayers hint to photochemically and microbially mediated DOM turnover in the upwelling region off the coast of Peru, *Biogeosciences*, 13, 2453–2473, <https://doi.org/10.5194/bg-13-2453-2016>, 2016.

Galletti, Y., Becagli, S., Di Sarra, A., Gonnelli, M., Pulido-Villena, E., Sferlazzo, D. M., Traversi, R., Vestri, S., and Santinelli, C.: Atmospheric deposition of organic matter at a remote site in the central Mediterranean Sea: implications for the marine ecosystem, *Biogeosciences*, 17, 3669–3684, <https://doi.org/10.5194/bg-17-3669-2020>, 2020.

Hansen, A. M., Kraus, T. E. C., Pellerin, B. A., Fleck, J. A., Downing, B. D., and Bergamaschi, B. A.: Optical properties of dissolved organic matter (DOM): Effects of biological and photolytic degradation, *Limnology & Oceanography*, 61, 1015–1032, <https://doi.org/10.1002/lno.10270>, 2016.

Hardy, J. T.: The Sea Surface Microlayer: Biology, Chemistry and Anthropogenic Enrichment, *Progress in Oceanography*, 11, 307–328, 1982.

Hardy, J. T.: Biological effects of chemicals in the sea-surface microlayer, in: *The Sea Surface and Global Change*, edited by: Liss, P. S. and Duce, R. A., Cambridge University Press, 339–370, <https://doi.org/10.1017/CBO9780511525025.012>, 2009.

Hardy, J. T. and Apts, C. W.: The sea-surface microlayer: phytoneuston productivity and effects of atmospheric particulate matter, *Mar Biol.*, 82, 293–300, <https://doi.org/10.1007/BF00392409>, 1984.

Harris, N. A., Sorensen, J. P. R., Marchant, B., Old, G. H., Naden, P. S., Bowes, M. J., Scarlett, P. M., Nicholls, D. J. E., Armstrong, L. K., Wickham, H. D., Read, D. S., Lapworth, D., Bond, T., and Pond, K.: Temporal drivers of tryptophan-like fluorescent dissolved organic matter along a river continuum, *Sci Total Environ.*, 928, <https://doi.org/10.1016/j.scitotenv.2024.172285>, 2024.



765 Helms, J. R., Stubbins, A., Ritchie, J. D., Minor, E. C., Kieber, D. J., and Mopper, K.: Absorption spectral slopes and slope ratios as indicators of molecular weight, source, and photobleaching of chromophoric dissolved organic matter, *Limnology and Oceanography*, 53, 955–969, <https://doi.org/10.4319/lo.2008.53.3.0955>, 2008.

770 Helms, J. R., Mao, J., Stubbins, A., Schmidt-Rohr, K., Spencer, R. G. M., Hernes, P. J., and Mopper, K.: Loss of optical and molecular indicators of terrigenous dissolved organic matter during long-term photobleaching, *Aquat Sci*, 76, 353–373, <https://doi.org/10.1007/s00027-014-0340-0>, 2014.

775 Huguet, A., Vacher, L., Relexans, S., Saubusse, S., Froidefond, J. M., and Parlanti, E.: Properties of fluorescent dissolved organic matter in the Gironde Estuary, *Organic Geochemistry*, 40, 706–719, <https://doi.org/10.1016/j.orggeochem.2009.03.002>, 2009.

Hunter, K. A.: Processes affecting particulate trace metals in the sea surface microlayer, *Marine Chemistry*, 9, 49–70, [https://doi.org/10.1016/0304-4203\(80\)90006-7](https://doi.org/10.1016/0304-4203(80)90006-7), 1980.

780 Hunter, K. A.: Chemistry of the sea-surface microlayer, in: *The Sea Surface and Global Change*, edited by: Liss, P. S. and Duce, R. A., Cambridge University Press, 287–320, <https://doi.org/10.1017/CBO9780511525025.010>, 2009.

Jaeger, L., Gassen, L., Ayim, S. M., Bibi, R., and Wurl, O.: Thermal Recovery Dynamics of the Ocean's Cool-Skin Layer After Complete Mixing, *Tellus A: Dynamic Meteorology and Oceanography*, 77, <https://doi.org/10.16993/tellusa.4103>, 2025.

785 Jibaja Valderrama, O., Scheres Firak, D., Schaefer, T., van Pinxteren, M., Fomba, K. W., and Herrmann, H.: Photochemistry of the sea-surface microlayer (SML) influenced by a phytoplankton bloom: A mesocosm study, <https://doi.org/10.5194/egusphere-2025-4066>, 1 January 2025.

Kieber, D. J., McDaniel, J., and Mopper, K.: Photochemical source of biological substrates in sea water: implications for carbon cycling, *Nature*, 341, 637–639, <https://doi.org/10.1038/341637a0>, 1989.

Kirk, J. T. O.: *Light and Photosynthesis in aquatic Ecosystems*, 3rd ed., Cambridge University Press, The Edinburgh Building, Cambridge CB2 8RU, UK, 665 pp., 1983.

790 Kothawala, D. N., Murphy, K. R., Stedmon, C. A., Weyhenmeyer, G. A., and Tranvik, L. J.: Inner filter correction of dissolved organic matter fluorescence, *Limnology & Ocean Methods*, 11, 616–630, <https://doi.org/10.4319/lom.2013.11.616>, 2013.

Kowalcuk, P., Tilstone, G. H., Zablocka, M., Röttgers, R., and Thomas, R.: Composition of dissolved organic matter along an Atlantic Meridional Transect from fluorescence spectroscopy and Parallel Factor Analysis, *Marine Chemistry*, 157, 170–184, <https://doi.org/10.1016/j.marchem.2013.10.004>, 2013.

Lawaetz, A. J. and Stedmon, C. A.: Fluorescence intensity calibration using the Raman scatter peak of water, *Appl Spectrosc*, 63, 936–40, <https://doi.org/10.1366/000370209788964548>, 2009.

795 Liebezeit, G., Thomas, K., and Beate, E.: Bulk chemical characterization of particulate material from the Jade Bay, Lower Saxonian Wadden Sea, *Netherlands Journal of Aquatic Ecology*, 28, 365–370, <https://doi.org/10.1007/BF02334206>, 1994.



Lilliefors, H. W.: On the Kolmogorov-Smirnov Test for Normality with Mean and Variance Unknown, *Journal of the American Statistical Association*, 62, 399–402, 1967.

Liss, P. S. and Duce, R. A. (Eds.): *The Sea Surface and Global Change*, 1st ed., Cambridge University Press, <https://doi.org/10.1017/CBO9780511525025>, 1997.

800 Lønborg, C., Álvarez-Salgado, X. A., Davidson, K., Martínez-García, S., and Teira, E.: Assessing the microbial bioavailability and degradation rate constants of dissolved organic matter by fluorescence spectroscopy in the coastal upwelling system of the Ría de Vigo, *Marine Chemistry*, 119, 121–129, <https://doi.org/10.1016/j.marchem.2010.02.001>, 2010.

805 Marcé, R., Verdura, L., and Leung, N.: Dissolved organic matter spectroscopy reveals a hot spot of organic matter changes at the river–reservoir boundary, *Aquat Sci*, 83, 67, <https://doi.org/10.1007/s00027-021-00823-6>, 2021.

Mason, J. D., Cone, M. T., and Fry, E. S.: Ultraviolet (250–550 nm) absorption spectrum of pure water, *Appl. Opt.*, 55, 7163, <https://doi.org/10.1364/AO.55.007163>, 2016.

McCarthy, M. D., Hedges, J. I., and Benner, R.: The chemical composition of dissolved organic matter in seawater, *Chemical Geology*, 107, 503–507, [https://doi.org/10.1016/0009-2541\(93\)90240-J](https://doi.org/10.1016/0009-2541(93)90240-J), 1993.

810 Miranda, M. L., Mustaffa, N. I. H., Robinson, T. B., Stolle, C., Ribas-Ribas, M., Wurl, O., and Zielinski, O.: Influence of solar radiation on biogeochemical parameters and fluorescent dissolved organic matter (FDOM) in the sea surface microlayer of the southern coastal North Sea, *Elem Sci Anth*, 6, 15, <https://doi.org/10.1525/elementa.278>, 2018.

Moran, M. A. and Zepp, R. G.: Role of photoreactions in the formation of biologically labile compounds from dissolved organic matter, *Limnology & Oceanography*, 42, 1307–1316, <https://doi.org/10.4319/lo.1997.42.6.1307>, 1997.

815 Murphy, K. R., Stedmon, C. A., Graeber, D., and Bro, R.: Fluorescence spectroscopy and multi-way techniques. PARAFAC, *Anal. Methods*, 5, 6557, <https://doi.org/10.1039/c3ay41160e>, 2013.

Murphy, K. R., Stedmon, C. A., Wenig, P., and Bro, R.: OpenFluor- an online spectral library of auto-fluorescence by organic compounds in the environment, *Anal. Methods*, 6, 658–661, <https://doi.org/10.1039/C3AY41935E>, 2014.

820 Mustaffa, N. I. H., Kallajoki, L., Hillebrand, H., Wurl, O., and Striebel, M.: Sea surface phytoplankton community response to nutrient and light changes, *Mar Biol*, 167, <https://doi.org/10.1007/s00227-020-03738-2>, 2020.

Nelson, N. B. and Siegel, D. A.: The Global Distribution and Dynamics of Chromophoric Dissolved Organic Matter // The global distribution and dynamics of chromophoric dissolved organic matter, *Ann Rev Mar Sci*, 5, 447–76, <https://doi.org/10.1146/annurev-marine-120710-100751>, 2013.

825 Nieto-Cid, M., Álvarez-Salgado, X. A., and Pérez, F. F.: Microbial and photochemical reactivity of fluorescent dissolved organic matter in a coastal upwelling system, *Limnol. Oceanogr.*, 51, 1391–1400, 2006.

Obernosterer, I., Catala, P., Reinthaler, T., Herndl, G. J., and Lebaron, P.: Enhanced heterotrophic activity in the surface microlayer of the Mediterranean Sea, *Aquat. Microb. Ecol.*, 39, 293–302, <https://doi.org/10.3354/ame039293>, 2005.

OpenAI: ChatGPT (GPT-5) [Large language model], 2025.

Parker, C. A. and Rees, W. T.: Fluorescence Spectrometry: A Review, 1962.



830 Peuravuori, J. and Pihlaja, K.: Molecular size distribution and spectroscopic properties of aquatic humic substances, *Analytica Chimica Acta*, 337, 133–149, [https://doi.org/10.1016/S0003-2670\(96\)00412-6](https://doi.org/10.1016/S0003-2670(96)00412-6), 1997.

Pinheiro and Bates: Fitting Nonlinear Mixed-Effect Models, in: *Mixed-Effects Models in Sand S-PLUS*. Statistics and Computing, Springer, New York, NY, 2000.

Rauch, C., Deyle, L., Jaeger, L., Cortés-Espinoza, E. F., Ribas-Ribas, M., Karnatz, J., Engel, A., and Wurl, O.:  
835 Phytoplankton blooms affect microscale gradients of oxygen and temperature across the sea surface microlayer, <https://doi.org/10.5194/egusphere-2025-4833>, 10 October 2025.

Reinthaler, T., Sintes, E., and Herndl, G. J.: Dissolved organic matter and bacterial production and respiration in the sea-  
surface microlayer of the open Atlantic and the western Mediterranean Sea, *Limnology and Oceanography*, 53, 122–136,  
https://doi.org/10.4319/lo.2008.53.1.0122, 2008.

840 Repetea, D. and Aluwihare, L.: Chemical characterization and cycling of dissolved organic matter, in: *Biogeochemistry of  
Marine Dissolved Organic Matter*, edited by: Hansell, D. A. and Carlson, C. A., Elsevier, 2024.

Retelletti Brogi, S., Charrière, B., Gonnelli, M., Vaultier, F., Sempéré, R., Vestri, S., and Santinelli, C.: Effect of UV and  
Visible Radiation on Optical Properties of Chromophoric Dissolved Organic Matter Released by *Emiliania huxleyi*, *JMSE*,  
8, 888, <https://doi.org/10.3390/jmse8110888>, 2020.

845 Rickard, P. C., Uher, G., and Upstill-Goddard, R. C.: Photo-Reactivity of Surfactants in the Sea-Surface Microlayer and  
Subsurface Water of the Tyne Estuary, UK, *Geophys. Res. Lett.*, 49, <https://doi.org/10.1029/2021GL095469>, 2022.

Rochelle-Newall, E., Delille, B., Frankignoulle, M., Gattuso, J. P., Jacquet, S., Riebesell, U., Terbruggen, A., and  
Zondervan, I.: Chromophoric dissolved organic matter in experimental mesocosms maintained under different pCO<sub>2</sub> levels,  
*Mar. Ecol. Prog. Ser.*, 272, 25–31, <https://doi.org/10.3354/meps272025>, 2004.

850 Roesler, C. S. and Barnard, A. H.: Optical proxy for phytoplankton biomass in the absence of photophysiology: Rethinking  
the absorption line height, *Methods in Oceanography*, 7, 79–94, <https://doi.org/10.1016/j.mio.2013.12.003>, 2013.

Romera-Castaño, C., Sarmento, H., Álvarez-Salgado, X. A., Gasol, J. M., and Marrasé, C.: Production of chromophoric  
dissolved organic matter by marine phytoplankton, *Limnology and Oceanography*, 55, 1466–1466,  
<https://doi.org/10.4319/lo.2010.55.3.1466>, 2010.

855 Röttgers, R., Doxaran, D., and Dupouy, C.: Quantitative filter technique measurements of spectral light absorption by  
aquatic particles using a portable integrating cavity absorption meter (QFT-ICAM), *Opt. Express*, 24, 1–20,  
<https://doi.org/10.1364/OE.24.0000A1>, 2016.

Röttgers, R., Novak, M. G., and Belz, M.: Measurement of light absorption by chromophoric dissolved organic matter using  
a type-II liquid capillary waveguide: assessment of an achievable accuracy, *Appl. Opt.*, 63, 3811–3824,  
860 <https://doi.org/10.1364/AO.516580>, 2024.

Shutova, Y., Baker, A., Bridgeman, J., and Henderson, R. K.: Spectroscopic characterisation of dissolved organic matter  
changes in drinking water treatment: From PARAFAC analysis to online monitoring wavelengths, *Water Research*, 54, 159–  
169, <https://doi.org/10.1016/j.watres.2014.01.053>, 2014.



Smith, D. J. and Underwood, G. J. C.: The production of extracellular carbohydrates by estuarine benthic diatoms: the  
865 effects of growth phase and light and dark treatment, *Journal of Phycology*, 36, 321–333, <https://doi.org/10.1046/j.1529-8817.2000.99148.x>, 2000.

Stedmon, C. A. and Bro, R.: Characterizing dissolved organic matter fluorescence with parallel factor analysis: a tutorial, *Limnology & Ocean Methods*, 6, 572–579, <https://doi.org/10.4319/lom.2008.6.572>, 2008.

Stedmon, C. A. and Markager, S.: Tracing the production and degradation of autochthonous fractions of dissolved organic  
870 matter by fluorescence analysis, *Limnol. Oceanogr.*, 50, 1415–1426, <https://doi.org/10.4319/lo.2005.50.5.1415>, 2005.

Stramski, D., Reynolds, R. A., Gernez, P., Röttgers, R., and Wurl, O.: Inherent optical properties and particle characteristics  
of the sea-surface microlayer, *Progress in Oceanography*, 176, 102117, <https://doi.org/10.1016/j.pocean.2019.05.009>, 2019.

Summers, R. S., Cornel, P. K., and Roberts, P. V.: Molecular size distribution and spectroscopic characterization of humic  
substances, *Sci Total Environ*, 62, 27–37, [https://doi.org/10.1016/0048-9697\(87\)90478-5](https://doi.org/10.1016/0048-9697(87)90478-5), 1987.

875 Thornton, D. C. O.: Dissolved organic matter (DOM) release by phytoplankton in the contemporary and future ocean,  
*European Journal of Phycology*, 49, 20–46, <https://doi.org/10.1080/09670262.2013.875596>, 2014.

Tilstone, G. H., Airs, R. L., Martinez-Vicente, V., Widdicombe, C., and Llewellyn, C.: High concentrations of mycosporine-  
like amino acids and colored dissolved organic matter in the sea surface microlayer off the Iberian Peninsula. *Limnol.*  
880 *Oceanogr.*, 55(5), 2010, 1835–1850, *Limnol. Oceanogr.*, 55, 1835–1850, <https://doi.org/10.4319/lo.2010.55.5.1835>, 2010.

Van Pinxteren, M., Barthel, S., Fomba, K. W., Müller, K., Von Tümpeling, W., and Herrmann, H.: The influence of  
environmental drivers on the enrichment of organic carbon in the sea surface microlayer and in submicron aerosol particles –  
measurements from the Atlantic Ocean, *Elementa: Science of the Anthropocene*, 5, 35, <https://doi.org/10.1525/elementa.225>,  
2017.

Verdugo, P.: Marine microgels, *Ann Rev Mar Sci*, 4, 375–400, <https://doi.org/10.1146/annurev-marine-120709-142759>,  
885 2012.

Walker, S. A., Amon, R. M. W., Stedmon, C., Duan, S., and Loucheouarn, P.: The use of PARAFAC modeling to trace  
terrestrial dissolved organic matter and fingerprint water masses in coastal Canadian Arctic surface waters, *J. Geophys. Res.*,  
114, 2009JG000990, <https://doi.org/10.1029/2009JG000990>, 2009.

Weishaar, J. L., Aiken, G. R., Bergamaschi, B. A., Fram, M. S., Fujii, R., and Mopper, K.: Evaluation of specific ultraviolet  
890 absorbance as an indicator of the chemical composition and reactivity of dissolved organic carbon, *Environ Sci Technol*, 37,  
4702–8, <https://doi.org/10.1021/es030360x>, 2003.

Wilson, T. W., Ladino, L. A., Alpert, P. A., Breckels, M. N., Brooks, I. M., Browse, J., Burrows, S. M., Carslaw, K. S.,  
Huffman, J. A., Judd, C., Kilthau, W. P., Mason, R. H., McFiggans, G., Miller, L. A., Nájera, J. J., Polishchuk, E., Rae, S.,  
Schiller, C. L., Si, M., Temprado, J. V., Whale, T. F., Wong, J. P. S., Wurl, O., Yakobi-Hancock, J. D., Abbatt, J. P. D.,  
895 Aller, J. Y., Bertram, A. K., Knopf, D. A., and Murray, B. J.: A marine biogenic source of atmospheric ice-nucleating  
particles, *Nature*, 525, 234–238, <https://doi.org/10.1038/nature14986>, 2015.



Wollschläger, J., Röttgers, R., Petersen, W., and Wiltshire, K. H.: Performance of absorption coefficient measurements for the in situ determination of chlorophyll-a and total suspended matter, *Journal of Experimental Marine Biology and Ecology*, 453, 138–147, <https://doi.org/10.1016/j.jembe.2014.01.011>, 2014.

900 Wurl, O., Miller, L., Röttgers, R., and Vagle, S.: The distribution and fate of surface-active substances in the sea-surface microlayer and water column, *Marine Chemistry*, 115, 1–9, <https://doi.org/10.1016/j.marchem.2009.04.007>, 2009.

Wurl, O., Miller, L., and Vagle, S.: Production and fate of transparent exopolymer particles in the ocean, *Journal of Geophysical Research*, 116, <https://doi.org/10.1029/2011JC007342>, 2011.

905 Wurl, O., Stolle, C., van Thuoc, C., The Thu, P., and Mari, X.: Biofilm-like properties of the sea surface and predicted effects on air-sea CO<sub>2</sub> exchange, *Progress in Oceanography*, 144, 15–24, <https://doi.org/10.1016/j.pocean.2016.03.002>, 2016.

Wurl, O., Ekau, W., Landing, W. M., and Zappa, C. J.: Sea surface microlayer in a changing ocean – A perspective, *Elementa: Science of the Anthropocene*, 5, <https://doi.org/10.1525/elementa.228>, 2017.

910 Wurl, O., Bird, K., Cunliffe, M., Landing, W. M., Miller, U., Mustaffa, N. I. H., Ribas-Ribas, M., Witte, C., and Zappa, C. J.: Warming and Inhibition of Salinization at the Ocean's Surface by Cyanobacteria, *Geophysical Research Letters*, 45, 4230–4237, <https://doi.org/10.1029/2018GL077946>, 2018.

Yang, L., Zhang, J., Engel, A., and Yang, G.-P.: Spatio-temporal distribution, photoreactivity and environmental control of dissolved organic matter in the sea-surface microlayer of the eastern marginal seas of China, *Biogeosciences*, 19, 5251–5268, <https://doi.org/10.5194/bg-19-5251-2022>, 2022.

915 Zäncker, B., Bracher, A., Röttgers, R., and Engel, A.: Variations of the Organic Matter Composition in the Sea Surface Microlayer: A Comparison between Open Ocean, Coastal, and Upwelling Sites Off the Peruvian Coast, *Front. Microbiol.*, 8, 2369, <https://doi.org/10.3389/fmicb.2017.02369>, 2017.

Zepp, R. G., Callaghan, T. V., and Erickson, D. J.: Effects of enhanced solar ultraviolet radiation on biogeochemical cycles, *Journal of Photochemistry and Photobiology B: Biology*, 46, 69–82, [https://doi.org/10.1016/S1011-1344\(98\)00186-9](https://doi.org/10.1016/S1011-1344(98)00186-9), 1998.

920 Zsolnay, A., Baigar, E., Jimenez, M., Steinweg, B., and Saccoccanti, F.: Differentiating with fluorescence spectroscopy the sources of dissolved organic matter in soils subjected to drying, *Chemosphere*, 38, 45–50, 1999.